Laboratory Experiments Bearing on the Origin and Evolution of Olivine-rich Chondrules

Frank M. Richter[1], Ruslan A. Mendybaev[1], John N. Christensen[2] , Denton Ebel[3], Amy Gaffney[4]
[1]Department of the Geophysical Sciences, University of Chicago
[2]Lawrence Berkeley National Laboratory
[3]American Museum of Natural History
[4]Lawrence Livermore National Laboratory

May 27, 2011

Corresponding author (richter@geosci.uchicago.edu)

Abstract

Evaporation rates of K_2O, Na_2O, and FeO from chondrule-like liquids and the associated potassium isotopic fractionation of the evaporation residues were measured to help understand the processes and conditions that affected the chemical and isotopic compositions of olivine-rich Type IA and Type IIA chondrules from Semarkona. Both types of chondrules show evidence of having been significantly or totally molten. However, these chondrules do not have large or systematic potassium isotopic fractionation of the sort found in the laboratory evaporation experiments. The experimental results reported here provide new data regarding the evaporation kinetics of sodium and potassium from a chondrule-like melt and the potassium isotopic fractionation of evaporation residues run under various conditions ranging from high vacuum to pressures of one bar of H_2+CO_2, or H_2, or helium. The lack of systematic isotopic fractionation of potassium in the Type IIA and Type IA chondrules compared with what is found in the vacuum and one-bar evaporation residues is interpreted as indicating that they evolved in a partially closed system where the residence time of the surrounding gas was sufficiently long for it to have become saturated in the evaporating species and for isotopic equilibration between the gas and the melt. A diffusion couple experiment juxtaposing chondrule-like melts with different potassium concentrations showed that the diffusivity of potassium is sufficiently fast at liquidus temperatures ($D_K > 2\times10^{-4} cm^2/s$ at 1650˚C) that diffusion-limited evaporation cannot explain why, despite their having been molten, the Type IIA and Type IA chondrules show no systematic potassium isotopic fractionation.

1. INTRODUCTION

Calcium-aluminum-rich inclusions (CAIs) and chondrules in chondritic meteorites have special importance in cosmochemistry because they provide unique information with which to deduce the conditions and processes that prevailed during the earliest stages of evolution of the solar system. CAIs are distinctive by being the oldest dated materials to have formed in the solar system while chondrules, which are typically 1 to 2 million years younger than the CAIs, are a major constituent of many types of chondritic meteorites. While this paper is mainly about laboratory experiments motivated by chondrules, a brief review of the conditions and processes that affected the CAIs will serve to highlight some major differences between what chondrules and what CAIs experienced in the protoplanetary disk. CAIs, while much less abundant than chondrules,

provide the more detailed story. Their major-element composition is made up almost entirely of MgO, CaO, SiO_2, and Al_2O_3 plus a small amount of TiO_2, in proportions that are close to what has been calculated for solids that would condense from a gas of solar composition cooled to about 1100˚C (Grossman, 1972). This suggests that CAIs are, or more likely that their precursors were, partial condensates that became isolated from the remaining gas either before the more volatile elements such as iron, sulfur, sodium, and potassium condensed or after these had re-evaporate by some later high temperature event. Many CAIs have distinctly igneous textures implying that their precursors were re-heated and melted by one or more high temperature events. In the case of the Type B CAIs, for example, peak temperatures must have been close to 1400˚C followed by cooling rates no greater than 50˚C/hr (Stolper and Paque, 1986; Richter et al., 2002; Mendybaev et al. 2006). The oxygen fugacity at the time of crystallization of the CAIs has been shown to be extremely reducing (Beckett, 1987, Beckett et al., 1988) indicating that the environment was still hydrogen-dominated, not much different from a gas of solar composition. CAIs often have correlated enrichments in the heavy isotopes of silicon and magnesium (Clayton et al, 1988) similar to what has been produced in laboratory vacuum evaporation experiments involving molten silicates (Davis et al., 1990; Wang et al., 2001; Richter et al., 2002, 2007; Knight et al., 2009). In view of these experiments, it is generally accepted that CAIs are enriched in the heavy isotopes of silicon and magnesium as a result of a fraction of their original silicon and magnesium having been lost by evaporation while the CAIs were molten or partially molten to a high degree. A plausible scenario for the origin and evolution of the Type B CAIs involves a precursor that condensed from a solar composition gas at about 1100˚C and that was then reheated to about 1400˚C producing a high degree of partial melting (about 95%). Cooling at 1-50 ˚C/hr from a peak temperature of about 1400˚C will have volatilized enough silicon and magnesium to account for the observed isotopic fractionations of the Type B CAIs. A detailed discussion and an example of how laboratory evaporation experiments are used to translate the observed texture and composition of Type B CAIs into a quantitative constraint on their thermal history is given in Richter et al. (2006).

Chondrules are small spherules, usually a millimeter or less in size, that are the major constituents of most chondritic meteorites. They are much more abundant and varied in composition and texture than CAIs (see reviews by Grossman and Wasson, 1983; Rubin, 2000; Zanda, 2004) and include elements such as iron, sodium and potassium that condense at much lower temperatures than those in CAIs. They are believed to be younger than CAIs by about 1-2 million years (see recent discussion by Villeneuve et al., 2009) and thus can give evidence of conditions at a somewhat more evolved stage of the protoplanetary disk. Many chondrules have textures that indicate that they were at some point partially or completely molten, which given the range of their bulk compositions would require reheating to temperatures 1350˚C to 1800˚C (Hewins and Radomsky, 1990; Radomsky and Hewins, 1990). While both CAIs and many types of chondrules show evidence of having been partially or entirely molten, a striking difference between them is that there is no significant isotopic fractionation of the most volatile components of the chondrules (Alexander et al., 2000; Galy et al., 2000; Alexander and Wang, 2001; Zhu et al., 2001; Alexander and Grossman, 2005). The contrast between the well-documented enrichment of the heavy isotopes of the more

volatile elements of CAIs and the lack of such an effect in chondrules raises a number of questions. Did significant amounts of potassium and/or iron evaporate from chondrules while they were partially molten? If not, why not? If yes, why is there no associated isotopic fractionation of potassium and/or iron? Broadly speaking, the differences in age, composition, and isotopic fractionation between chondrules and CAIs imply that they had different precursors that evolved in very different environments (i.e., different surrounding gas and/or different temperature histories). To be more specific, however, requires a detailed consideration of the composition of particular types of chondrules interpreted using thermodynamic and experimental data on the evaporation kinetics and associated elemental and isotopic fractionations of volatile components from chondrule-like melts under a variety of plausible conditions.

The main focus of the present paper is to report new laboratory data on the evaporation rates of K_2O, Na_2O, and FeO from chondrule-like liquids and the associated potassium isotopic fractionation of the evaporation residues under different conditions. These data are used to discuss the elemental and isotopic compositions of olivine-rich Type IA and Type IIA chondrules from Semarkona, which show evidence of having been significantly or totally molten. The experimental data on the K_2O-Na_2O-FeO evaporation trajectories of molten chondrule-like compositions is used to address the more specific question of whether different degrees of volatilization starting from a common precursor can reproduce observed variations in K_2O, Na_2O, and FeO in Semarkona Type IA and Type IIA chondrules. Data from laboratory vacuum evaporation experiments are combined with thermodynamic calculations to discuss whether the duration of the transient heating and partial melting event as inferred from chondrule textures (see Tables 1 and 2 in Desch and Connolly, 2002) could have been sufficiently short for little or no evaporation to have taken place. The elemental and isotopic compositions of residues evaporated into vacuum and into one bar of slowly flowing gases of different composition document conditions where elements such as potassium can be volatilized with different degrees of associated isotopic fractionation. New experimental data on the rate of potassium diffusion in chondrule-like melts are used to evaluate the idea (Young, 2000) that the lack of significant isotopic fractionation could have been due to diffusion-limited evaporation.

A major part of the present study was to determine the isotopic fractionation of potassium in vacuum evaporation residues. This was motivated in part by the fact that earlier evaporation studies (Yu et al., 2003; Cohen et al. 2004) reported a wide range of different and puzzling results for potassium isotopic fractionations versus the amount of potassium volatilized. One set of experiments by Yu et al. (2003) showed the surprising result of kinetic isotope fractionation factors for potassium greater than the inverse square root of the isotope masses. The other Yu et al. (2003) experiments reported isotopic fractionations of the evaporation residues that would first increase and then decrease back towards the starting isotopic composition with increasing potassium evaporated. Yu et al. (2003) acknowledged that their potassium evaporation experiments were affected to varying degrees by experimental artifacts. Our new evaporation experiments were conceived to test whether the kinetic isotope fractionation of potassium evaporated from a chondrule-like liquid into vacuum would produce a Rayleigh-fractionated residue (i.e.,

increasing isotope fractionation with increasing evaporation) with an effectively constant kinetic isotope fractionation factor. Rayleigh fractionation behavior has been found for magnesium, silicon, and iron in all our earlier vacuum evaporation experiments (Richter et al., 2002 and 2007; Dauphas et al., 2004; Knight et al. 2009). Richter et al. (2002) and Knight et al. (2009) also showed that the kinetic isotope fractionation of CAI-like liquids by evaporation into a low-pressure hydrogen-dominated gas ($P=1.87\times10^{-4}$ bars) is very much the same as into vacuum even though the evaporation rate at this hydrogen pressure is orders of magnitude faster than in vacuum. An important natural example of Rayleigh-like potassium isotopic fractionation by evaporation was reported by Taylor et al. (2005) in their study of the elemental and isotopic fractionations of cosmic spherules. New evaporation experiments were also run in a one-bar gas-mixing furnace where molten chondrule-like compositions were exposed to a slowly flowing gas stream. Under these conditions the evaporation residues become progressively depleted in sodium, potassium and sometimes iron, but the degree of associated isotopic fractionation is very much dependent on the composition of the surrounding gas and how the gas is removed from the vicinity of the evaporating sample.

In the next section we review some general aspects of the compositional data of Type IIA chondrules from Semarkona (data from Jones, 1990 and Alexander et al., 2008) and from Type IA chondrules also from Semarkona (Jones and Scott, 1989). We use the data from Alexander and Grossman (2005) in our discussion of the isotopic composition of the Semarkona chondrules. This is followed by a section describing the procedures and results of the laboratory experiments used to determine the elemental and isotopic fractionation associated with evaporation of chondrule-like melts. In the final section, the chemical and isotopic data from the Semarkona chondrules are interpreted in light of the experimental results for the evaporation kinetics and kinetic isotope fractionations of chondrule-like liquids to make inferences regarding the conditions and processes that were experienced by these particular types of chondrules.

2. SEMARKONA CHONDRULES

Much of the motivation and discussion of the experimental work we report involves the chemical and isotopic compositions of the volatile components of chondrules from the unequilibrated ordinary chondrite Semarkona (LL3.0). Figure 1 shows the solar composition-normalized average chemical compositions of selected oxides in Type IIA (FeO-rich) and Type IA (FeO-poor) chondrules from Semarkona. The figure shows that with the exception of iron, the elemental abundances in Type IIA chondrules are on average relatively unfractionated regardless of volatility when compared to bulk solar system abundances, which has been used to argue that they formed and evolved in what was to first order a closed system for the major components except iron (see discussion of chondrites and their components by Scott and Krot, 2007 and references therein). The depletion in FeO is often interpreted to be the result of an iron metal component having either condensed separately or mechanically separated from the now silicate-dominated chondrule. Ebel and Grossman (2000) suggested that "sequestrations" of Ca-, Al-rich condensates might have played a role in producing the

slight excesses of SiO_2 and MgO relative to the more refractory Al_2O_3 and CaO seen in the averaged Type IIA data shown in Fig. 1, but this enrichment is small and could easily be a sampling artifact. The somewhat larger enrichment of the volatile Na_2O and K_2O components relative to refractory Al_2O_3 could be an indication that recondensation from a volatile-rich gas played a role. In contrast to the Type IIA chondrule compositions, Type IA chondrules are significantly depleted in Na_2O and K_2O, and much more depleted in FeO, which has been taken to imply volatile loss from an open system (see again the recent discussion by Scott and Krot, 2007).

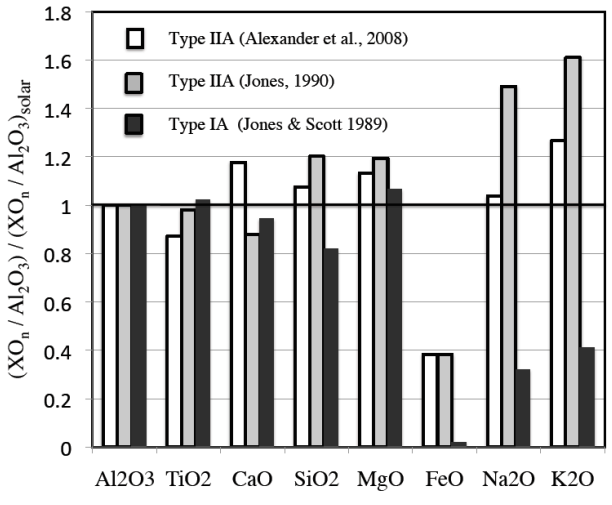

Figure 1. Average bulk composition of Semarkona chondrules using data reported by Alexander et al. (2008) for Type IIA chondrules, by Jones (1990) for different set of Type IIA chondrules and by Jones and Scott (1989) for Type IA chondrules. The wt% of the oxides is relative to that of Al_2O_3 and normalized by the solar ratio of the oxides using the abundances given by Palme and Jones (2004).

The data shown in Fig. 1 are averages and as such hide a great deal of interesting correlations between the various oxide components of the individual Semarkona chondrules. An example of this is shown in Fig. 2 in terms of the correlation between the wt% K_2O and wt% Na_2O of the bulk compositions of the Type IIA Semarkona chondrules. The dashed line in the figure corresponds to the solar ratio of these two oxides and the trend of the data shows a similar slope, with potassium being in most cases slightly enriched relative to sodium. At first sight, the trend of the data in Fig. 2 would seem to suggest that the sodium and potassium, being similarly volatile, might have evolved in an open system becoming enriched by condensation or depleted by evaporation in some fixed proportion.

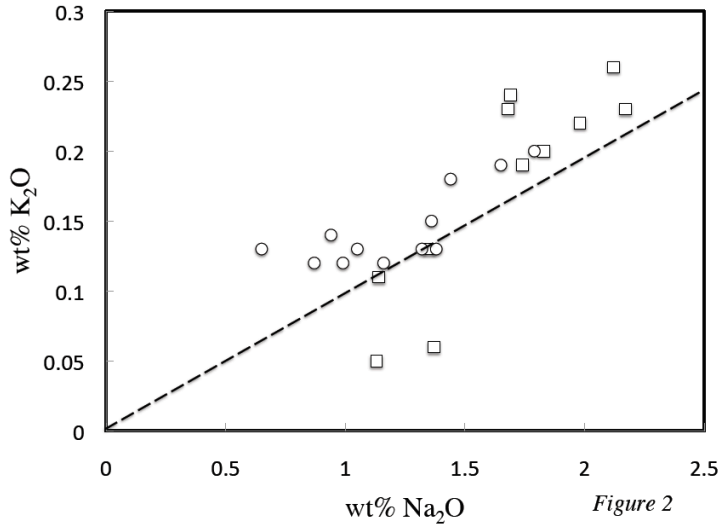

Figure 2. Wt% K_2O vs. wt% Na_2O of the bulk composition of individual Type IIA chondrules as reported by Jones, 1990 (square symbols) and by Alexander et al., 2008 (circles). The dashed line corresponds to the wt% ratio of these two oxides for a solar bulk composition.

Interpreting the co-variation of potassium and sodium seen in Fig. 2 as arising from the similar volatility of these two elements, as was done by Richter et al. (2009a), becomes problematic, if not untenable, once one considers how these abundances also co-vary with other much less volatile elements. An example of this is shown in Fig. 3 where much of the variation in the wt% of Na_2O and K_2O is seen to correlate with changes in the wt% of Al_2O_3, which being the most refractory of the major oxide components in chondrules would be expected to have fully condensed and not to have been affected by any later evaporation. The dashed line in Fig. 3 has a slope corresponding to the solar ratio of Na_2O/Al_2O_3 and $10.2\times$wt% K_2O/Al_2O_3. The factor 10.2 multiplying the wt% K_2O corresponds to the ratio of wt%Na_2O/wt%K_2O for the solar abundances given by Palme and Jones (2004) and thus multiplying the wt% K_2O by this factor allows it to be plotted on the same scale as Na_2O and show the degree to which they are in solar proportions. The fact that a significant fraction of the sodium and potassium data plot above the dashed line implies an enrichment of volatiles in the bulk compositions of many of the Semarkona chondrules as was already shown in Fig. 1. The general pattern of increasing Na_2O or K_2O with increases in the very refractory Al_2O_3 cannot have resulted from evaporation or condensation.

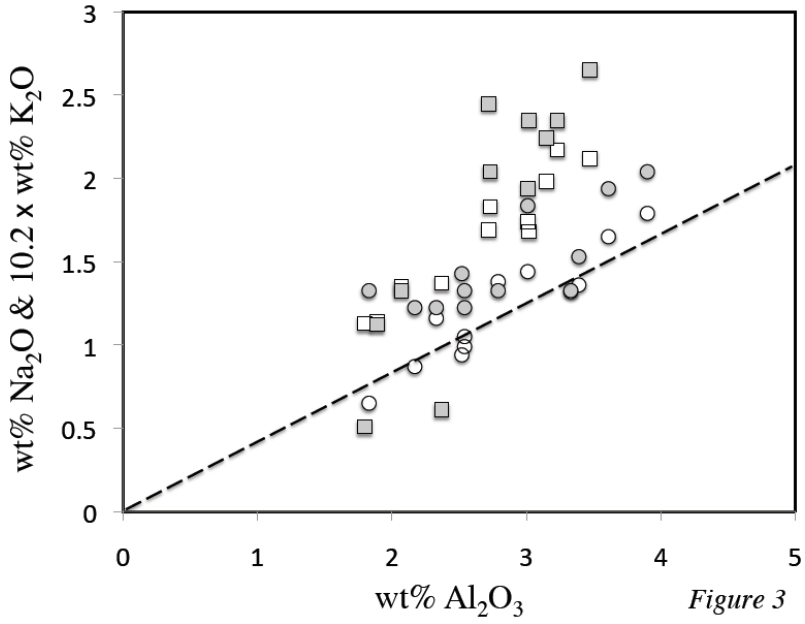

Figure 3. Wt% Na_2O (open symbols) and 10.2×wt%K_2O (filled symbols) of the bulk composition of Type IIA Semarkona chondrules plotted against the wt% Al_2O_3. The factor 10.2 multiplying the wt% K_2O is the ratio of the weight percents of Na_2O to K_2O in bulk solar system (Palme and Jones, 2004) and is used so that the abundance of these oxides in a given chondrule would plot on top of each other if they have exactly solar proportions. The dashed line corresponds to the solar ratio of wt% Na_2O and 10.2×wt% K_2O to wt% Al_2O_3. The chondrule data plotted as squares are from Jones (1990) and those plotted as circles are from Alexander et al., (2008).

Figure 4 shows that when the bulk compositions of Type IIA chondrules reported by Jones (1990) and Alexander et al. (2008) are considered separately in a plot of wt%K_2O/wt%Al_2O_3 versus wt%Na_2O/wt%Al_2O_3 they tend to cluster with little if any evidence of volatility-related fractionation. This together with the fact that there are significant variations in Na_2O abundance which are highly correlated with that of the much more refractory Al_2O_3 component (Fig. 3) implies that these variations reflect a heterogeneous set of precursors and that the Type IIA chondrules could well have remained closed systems even while molten. Zoning profiles in minerals from Type II chondrules have also been used to argue for closed system crystallization (Jones, 1990; Jones and Lofgren; 1993, Alexander et al., 2008; Borisov et al., 2008). Olivine is the liquidus phase for Type IIA compositions, and thus the fact that measurable sodium was found in the olivine cores (as shown in Fig. 1 of Alexander et al. 2008 and implied by data in their Table 1) is clear evidence that there was sodium in the melt at liquidus temperature (T>1600˚C) even though at these temperatures sodium would be expected to evaporate in a matter of seconds. The overall conclusion is that the Type IIA chondrules considered here had precursors with more or less solar proportions of the major oxides except for a deficit of about 50% in wt% FeO_2 and enrichments of up to 50% or more in the wt % of K_2O (and somewhat less for Na_2O) relative to the more refractory oxides, and that these chondrules remained effectively closed systems despite their having been melted to a high degree or even entirely.

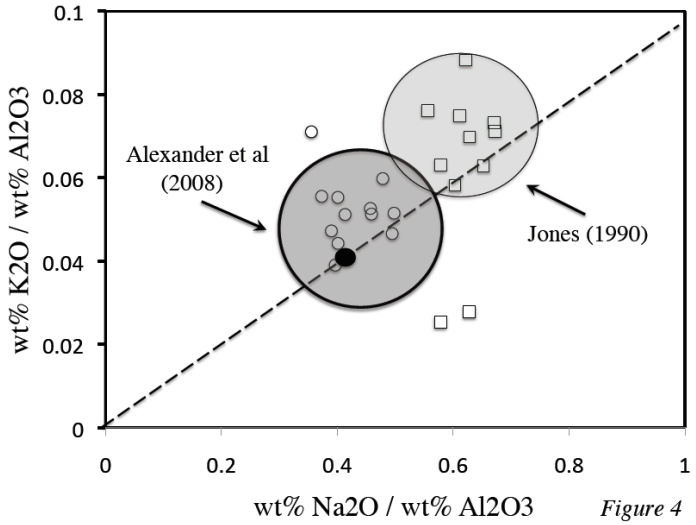

Figure 4. Plot of the wt%K_2O/wt%Al_2O_3 versus wt%Na_2O/wt%Al_2O_3 of individual Semarkona Type IIA chondrules showing that the data from Jones, 1990 (squares) and that of Alexander et al., 2008 (circles) tend for the most part to cluster as indicated by the two shaded circles. Within each cluster there is little if any evidence of variable loss of volatile sodium and potassium relative to the much more refractory aluminum. The dashed line is the correlation line for materials having solar proportions of K_2O and Na_2O. The small black circle indicates the ratio of wt%K_2O/wt%Al_2O_3 and wt%Na_2O/wt%Al_2O_3 for the solar abundances given by Palme and Jones (2004).

The average bulk composition of the Type IA chondrules reported by Jones and Scott (1989) is, as was already shown in Fig. 1, quite different from that of the Type IIA chondrules in terms of the abundance of FeO, K_2O, and Na_2O relative to Al_2O_3. This marked difference can also be seen when individual Type IA chondrule data are plotted in Fig. 5 in the same way as was done for the Type IIA chondrules in Fig. 3. While most of the Type IIA chondrules are somewhat enriched in sodium and potassium relative to aluminum compared to bulk solar proportions, the Type IA chondrules analyzed by Jones and Scott (1989) are in most cases significantly depleted in sodium and potassium relative to aluminum. The fact that the Na_2O and K_2O data points in Fig. 5 for a given wt% Al_2O_3 are close to each other is an indication that they are also close to being in solar proportions. Contrary to what was shown in Fig. 3 for the Type IIA chondrules, the wt% Na_2O and K_2O of the Type IA chondrules, except for two, are not obviously correlated with the wt% of Al_2O_3. Figure 6, which is the equivalent of Fig. 4 but for Type IA chondrules, shows the degree to which the wt% Na_2O and wt% K_2O correlate with a slope close to that of the solar ratio of these oxide components. This correlation could be an indication that the Types IA chondrules had a common precursor and that their present bulk compositions reflect different degrees of volatile loss by evaporation.

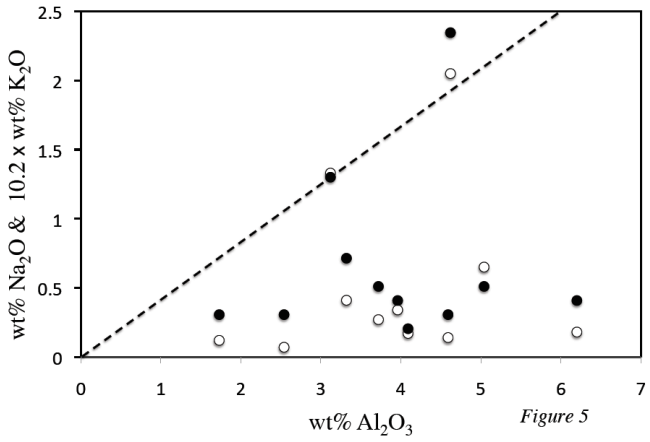

Figure 5. Same as Fig. 3 but for the Type IA chondrule compositions reported by Jones and Scott (1989). The wt% Na_2O (open circles) and 10.2 times the wt% K_2O (filled circles) are plotted against the wt% Al_2O_3 of the individual chondrules. The dashed line corresponds to the locus of point with solar proportions of Na_2O or $10.2\times K_2O$ to Al_2O_3.

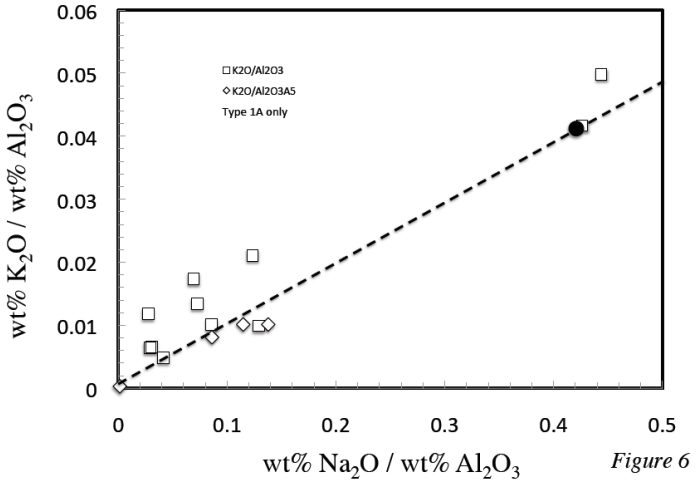

Figure 6. Similar to Fig. 4 but now for the bulk composition of Type IA chondrules reported by Jones and Scott, 1989 (square symbols) and Alexander and Grossman, 2005 (diamond symbols). The black circle indicates the wt%Na_2O/wt%Al_2O_3 and wt%K_2O/wt%Al_2O_3 of bulk solar system material as given by Palme and Jones (2004).

The above discussion focused mainly on the sodium and potassium compositions of the Type IA and Type IIA chondrules from Semarkona. These two types of chondrule are very different in their iron content (see Fig. 1), which Cohen et al. (2004) suggested could be due to the Type IA chondrules having evolved from the Type IIA chondrules by evaporation. They advocated for such a relationship based on experiments showing that a CI initial composition could, with increasing volatilization, evolve to a bulk composition similar to that of the Type II and Type I chondrules. Cohen et al. (2004) did note a key difficulty with this idea in that there is still measurable sodium and potassium present in actual chondrules. Because sodium and potassium are much more volatile than iron it is

hard to understand how they would not have fully evaporated long before any significant fraction of iron had volatilized. Furthermore, large systematic isotopic fractionations of volatile or moderately volatile elements have not been found in chondrules (see Galy et al., 2000 for magnesium, Alexander and Wang, 2001 for iron; Alexander et al., 2000 and Alexander and Grossman, 2005 for potassium), which would appear to be a further argument against significant evaporation in excess of recondensation.

For present purposes, the lack of significant isotopic fractionation of potassium is especially relevant. In this connection, it is worth noting that while the reported potassium isotopic composition of chondrules for Bishunpur (Alexander et al., 2000) and Semarkona (Alexander and Grossman, 2005) do not show simple systematics with respect to possible measures of potassium depletion, such as K/Al ratios, they are in many cases significantly fractionated compared to the reported analytical precision. The authors did acknowledge that their stated error estimates might significantly underestimate the true uncertainly of the potassium isotopic composition. Figure 7 shows the potassium isotopic composition of Type IA and Type IIA chondrules from Semarkona plotted against their potassium abundance relative to aluminum.

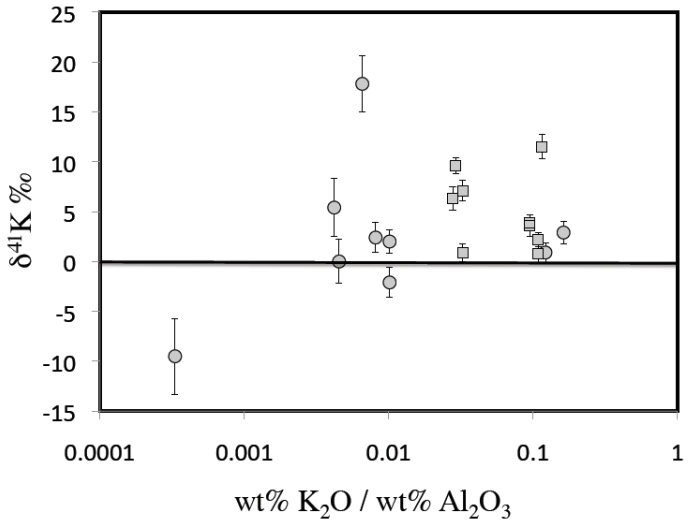

Figure 7. Potassium isotopic composition and 2σ error bars of Semarkona Type IIA (square symbols) and Type IA (circles) chondrules reported by Alexander and Grossman (2005). The potassium isotopic composition is reported as $\delta^{41}K\text{‰} \equiv 1000 \times \left(\frac{(^{41}K/^{39}K)_{sample}}{(^{41}K/^{39}K)_{std}} - 1 \right)$.

Figure 7 shows that the published data and associated errors of the potassium isotopic composition of Type IA and Type IIA chondrules do not support the common claim that chondrules are not fractionated in potassium isotopes. What can be said is that the isotopic fractionations of potassium in chondrules are small compared to specific expectations such as perfect open-system Rayleigh fractionation by evaporation. There is only one chondrule with an isotopic composition that might suggest non-equilibrium

recondensation of potassium, which would be isotopically light. Furthermore a larger fraction of the Type IIA chondrules are heavy in potassium isotopic composition compared to the Type IA chondrules. If significant, this difference is opposite what one would expect if the relative depletion of potassium of the Type IA chondrules compared Type IIA (see Figures 1 and 5) were due to kinetic isotope fractionation by evaporation.

3. THEORETICAL CONSIDERATIONS

Silicate materials held at or near their solidus temperature in a low-pressure environment for a sufficiently long time will lose some fraction of the more volatile elements relative to the more refractory ones. The usual parameterization of the evaporation rate of a given component is the Hertz-Knudsen equation (see Hirth and Pound, 1963)

$$J_i = \frac{\gamma_i (P_i^{sat} - P_i)}{\sqrt{2\pi m_i RT}} \tag{1}$$

where J_i is the flux of element or isotope i in moles per unit area per unit time, γ_i is an empirical evaporation coefficient, P_i^{sat} is the equilibrium vapor pressure of i and P_i is the pressure of i at the evaporating surface, m_i is the molecular mass of the gas molecule containing i, R is the gas constant, and T is absolute temperature. Equation (1) is strictly valid in the limit of a single dominant gas molecule containing i, and for that gas molecule having only one atom of i. This is the case for sodium and potassium because the gas in equilibrium with a chondrule-like liquid will for the most part contain monoatomic Na and K. Equation (1) also implicitly assumes that the recondensation rate when there is a finite vapor pressure at the surface depends on a recondensation coefficient that is effectively the same as the evaporation coefficient γ_i. The evaporation and condensation coefficients must be equal at least as P_i approaches P_i^{sat} in order that the net evaporation rate go to zero once the surface pressure of i equals the saturation vapor pressure. There is no theory for specifying γ_i in the case of silicate liquids, thus laboratory experiments are required for determining the value of the evaporation coefficients to be used in Eqn. (1).

Of special interest for present purposes are trajectories in Na_2O-K_2O-FeO space. In the limiting case of no recondensation, Eqn. (1) can be used to calculate trajectories. In the case of sodium and potassium, for example, the trajectory is given by

$$\frac{J_{Na}}{J_K} = \frac{\gamma_{Na} P_{Na}^{sat}}{\gamma_K P_K^{sat}} \sqrt{\frac{m_k}{m_{Na}}} \tag{2}$$

where the values used for the mass are those of the dominant gas species that would be in equilibrium with the silicate liquid. Thermodynamic calculations of the speciation of gas in equilibrium with chondrule-like liquids show that the dominant gas species are

monoatomic potassium, sodium, and iron. A similar equation can be used for the flux of an alkali element relative to that of iron. Equation (2) is specifically for kinetic evaporation in the limit of no recondensation (i.e., $P_i / P_i^{sat} = 0$). The net evaporation flux, $J_{i,net}$, in the more general case of evaporation into a stagnant surrounding gas of finite total pressure was given by Richter et al. (2002) as

$$J_{i,net} = \frac{J_i\left(1 - \frac{P_{i,\infty}}{P_i^{sat}}\right)}{1 + \frac{\gamma_i a}{D_i}\sqrt{\frac{RT}{2\pi m_i}}} \qquad (3)$$

where J_i is the free evaporation rate as given by Eqn. (1) with P_i=0, $P_{i,\infty}$ is the far-field pressure of i not yet affected by evaporation, a is the radius of the evaporating source assumed to be a sphere, and D_i is the diffusion coefficient of i in the surrounding gas. This equation takes into account recondensation due to the finite surface pressure that must be greater than the far field pressure in order for the evaporating species to diffuse away from the surface through the stagnant surrounding gas. Richter et al. (2002) suggested that a reasonable choice for the dependence of D_i on temperature and total surrounding pressure is $D \approx \frac{0.00014}{P_{total}} T^{3/2}$ (total pressure in bars and the diffusion coefficient in units of cm^2/sec). Equation (3) shows that the limit of free evaporation requires both that $P_{i,\infty} << P_i^{sat}$ and that the total pressure be sufficiently low that the diffusivity is large enough so that $\frac{\gamma_i a}{D_i}\sqrt{\frac{RT}{2\pi m_i}} << 1$. If there is significant flow of the surrounding gas around the molten sphere, the conditions for free evaporation are less demanding.

There is one other limiting situation that will be relevant to the results of the laboratory experiments discussed in later sections. This is the limit of evaporation into a surrounding gas that is being removed from the system sufficiently slowly such that gas has had a chance to equilibrate with the condensed phase. In these circumstances the elemental and isotopic fractionations will depend on whether the volatilized species are being removed by advection (i.e., the flow of saturated gas) or by diffusion in the gas. The relevant equations for this case are derived in an Appendix.

The Hertz-Knudsen equation can be used to construct an equation for the isotopic composition of the evaporation flux, which is illustrated below for potassium isotopes in the limit of free evaporation (i.e., $P_K << P_K^{sat}$) and negligible equilibrium isotope fractionation.

$$\frac{J_{^{41}K}}{J_{^{39}K}} = \frac{\gamma_{41} P^{sat}_{^{41}K}}{\gamma_{39} P^{sat}_{^{39}K}} \sqrt{\frac{39}{41}} = \left(\frac{^{41}K}{^{39}K}\right)_{melt} \frac{\gamma_{41}}{\gamma_{33}} \sqrt{\frac{39}{41}} \qquad (4)$$

where $\frac{P^{sat}_{^{41}K}}{P^{sat}_{^{39}K}} = \left(\frac{^{41}K}{^{39}K}\right)_{melt}$ is used based on the assumption of no equilibrium isotope fractionation, which is generally assumed given the high temperature of silicate melts. Equation (4) shows that the isotopic composition differs from that of the evaporation source by a kinetic isotope fractionation factor $\frac{\gamma_{41}}{\gamma_{39}} \sqrt{\frac{39}{41}}$. Laboratory vacuum evaporation experiments are required for determining the quantity $\frac{\gamma_{41}}{\gamma_{39}}$, which cannot be assume to be exactly one for potassium given that it is not equal to one for magnesium, silicon, and iron isotopes evaporated from molten silicates (see Davis et al., 1990; Wang et al., 2001; Richter et al., 2002, 2007; Dauphas et al., 2004; Knight et al., 2009).

The usual representation for the isotopic fractionation of evaporation residues as a function of the amount of material evaporated is the Rayleigh fractionation equation, which for potassium isotopes becomes

$$\frac{(^{41}K/^{39}K)}{(^{41}K/^{39}K)_O} = (f_{^{39}K})^{\alpha_K - 1} \qquad (5)$$

where $(^{41}K/^{39}K)$ is the isotopic composition of the residue, $(^{41}K/^{39}K)_O$ is the initial isotopic composition of the condensed phase, $f_{^{39}K}$ is the fraction of ^{39}K remaining in the residue, and the kinetic isotope fractionation factor is $\alpha_K = \frac{\gamma_{41}}{\gamma_{39}} \sqrt{\frac{39}{41}}$. Equation (5) assumes that the condensed phase remains effectively well mixed (i.e., homogeneous) during evaporation, which will be the case when chemical diffusion in the melt is fast compared to the rate at which material is being lost from the surface. It also requires that α_K be effectively unchanging despite the evolving composition of the condensed phase (see Richter, 2004 for a detailed derivation of Eqn. (5) and further discussion of the conditions when it can be used for evaporation residues). For the purpose of testing whether the isotope fractionation of a set of residues evaporated to varying degrees from a common starting composition corresponds to Rayleigh fractionation, Eqn. (5) is restated by taking the logarithm of both sides such that

$$\ln\left(\frac{(^{41}K/^{39}K)_{sample}}{(^{41}K/^{39}K)_o}\right) = -(1 - \alpha_K)\ln(f_{^{39}K}) \qquad (6)$$

α_K is then evaluated using the slope $(1-\alpha_K)$ defined by the composition of the residues plotted as $\ln\left(\frac{(^{41}K/^{39}K)_{sample}}{(^{41}K/^{39}K)_o}\right)$ versus $-\ln(f_{^{39}K})$.

Equation (3) shows how recondensation due to a finite surface pressure reduces the net evaporation rate. Recondensation will also reduce the degree of isotopic fractionation associated with a given amount of element removed by evaporation. Richter et al. (2002) derived the following relationship between the effective isotope fractionation factor α' (finite P_i) and α (limit P_i=0) for isotopes 1 and 2 of element *i*.

$$\alpha' - 1 = (\alpha - 1)\left(1 - \frac{P_i}{P_i^{sat}}\right) + \left(\frac{D_{i,1}}{D_{i.2}} - 1\right)\frac{P_i}{P_i^{sat}} \qquad (7)$$

where $D_{i,1}$ and $D_{i,2}$ are the diffusion coefficients of isotopes 1 and 2 in the gas surrounding the evaporating source. Figure 13 in Richter et al. (2002) shows that at low surrounding gas pressure (P<10^{-3} bars) $P_i/P_i^{sat} \to 0$ and $\alpha' \to \alpha$, but that as the surrounding pressure become of the order of one bar, $P_i/P_i^{sat} \to 1$ and $\alpha' \to D_{i,1}/D_{i,2}$. Thus as a function of surrounding gas pressure the kinetic isotope fractionation goes from being determined by surface evaporation to controlled by diffusion in the surrounding gas.

The derivation leading to Eqn. (4) assumes that the isotope fractionation between a melt in equilibrium with surrounding gas is negligibly small. We attempted to test this assumption by experiments in which a silicate melt is exposed to a sufficiently slowly flowing gas in a vertical tube furnace such that the gas in the furnace is effectively in equilibrium with the melt. The idea was that as the gas saturated in the volatile elements is continuously removed from the system, the melt would become depleted in these elements in proportion to their relative saturation vapor pressures. Furthermore, we expected that there would be no measurable isotopic fractionation of residues of melts evaporated at slow flow rates in the tube furnace experiments because the equilibrium isotope fractionations at liquidus temperatures would be negligible. To our surprise, we found that the evaporation residues run in the tube furnace were still measurably fractionated in their isotopic composition. We finally realized that what we were measuring was most likely the isotopic fractionation of gas species due to diffusion in the furnace gas, and showed this to be the case by demonstrating how this fractionation varied when we changed the mean molecular weight of the furnace gas. The equations that apply to evaporation in a one-bar tube furnace where gas is continuously being removed are given in an Appendix.

Several recent papers have considered diffusion-limited evaporation as a way of suppressing isotope fractionation during evaporation (Young, 2000, Galy et al., 2000). Diffusion-limited evaporation arises when the evaporation rate is sufficiently fast that chemical diffusion is unable to maintain the homogeneity of the condensed phase. When a multi-component evaporating system is diffusion-limited, both the evaporation rate and the associated isotopic fractionation of the residue are suppressed. The quantity

determining whether or not a system will be diffusion limited during evaporation is the ratio of the diffusive equilibration times scale to the time scale over which evaporation would remove the element of interest. Richter et al. (2002) used this ratio of time scales to define a parameter they called the evaporation number for component i, $E_{vi} = 3J_i r / C_i D_i$, where J_i is the evaporation rate, r is the radius of the evaporating object assumed to be a sphere, C_i is the molar concentration of i in the condensed phase, and D_i is the diffusion coefficient of i in the melt. An evaporating system will be significantly diffusion-limited if $E_{vi} >> 1$ (see Fig. 14 in Richter et al. 2002). Combining experimental data on the evaporation rate of a given component with the diffusivity of that component in the condensed phase will allow for an estimate of whether or not the evaporation of potassium from a chondrule melt would have been diffusion limited.

4. EXPERIMENTAL AND ANALYTICAL METHODS

4.1 Sample Compositions

Several chondrule-like starting materials (Table1) were used for the evaporation experiments. The IIAB1 starting composition is similar to the composition used by Yu et al. (2003) in their study of potassium evaporation from a chondrule-like liquid. The potassium concentration in the IIAB1 composition (~3 wt% K_2O) is about a factor of ten higher than that of natural Type IIA chondrules (see Fig. 2), while the wt% FeO is between that of typical Type IIA chondrules (~15 wt%) and Type IA (~2 wt%) chondrules. The high potassium concentration of this starting composition allowed for high-precision potassium isotopic analyses of even the most highly evaporated residues. The Type IIAB2 composition (~0.02 wt% K_2O) was used to determine the composition trajectory in Na_2O-K_2O space and evaporation rates of residues that started with a more realistic ratio of K_2O to Na_2O. The potassium-enriched composition IIAB5 was used in evaporation experiments for measuring the potassium isotopic composition of residues run in one bar of H_2+CO_2. Evaporation experiments were also run in one-bar of hydrogen or helium (50Di50Le series) using a starting composition enriched in potassium and without iron or sodium.

4.2 Vacuum Evaporation Experiments

Powders of the starting materials together with a small amount of polyvinyl alcohol as a binder were placed onto 2.5 mm iridium wire loops, dried for at least 10 hours, and then placed in a one-bar furnace at 1000°C for 5 min in air to sinter the powder and to remove the polyvinyl alcohol. The samples were then suspended in a vacuum furnace (P~10^{-6} Torr), the furnace temperature raised to 1470˚C and held at this temperature for varying lengths of time. A description of the vacuum furnace is given in Hashimoto (1990) and the detailed experimental procedure in Richter et al. (2007). Both potassium and sodium are sufficiently volatile that there will be some loss of these elements while the samples are being heated to the run temperature and during the time it takes for the sample to cool after the power to the heating elements is shut down. For this reason we use the zero time runs, where power to the heaters was shut down as soon as

the temperature reached the run temperature, as the effective starting composition for determining the evaporation rates and isotopic fractionation of potassium.

4.3 One-bar Hydrogen Evaporation Experiments

The initial one-bar experiments involved evaporation into a slowly flowing stream of H_2-CO_2 gas in a vertical gas-mixing Deltech tube furnace similar in design to that described by Williams and Mullins (1976). The oxygen fugacity at the sample was maintained by adjusting the H_2-CO_2 mixture flowing into the furnace tube and monitored using a Y_2O_3-doped zirconia oxygen fugacity probe (see Mendybaev et al., 1998 for calibration of this probe). The experiments were conducted at oxygen fugacities 2.5 log units above that of the iron-wüstite (IW) buffer (log fO_2 = IW+2.5) to keep iron in the oxidized form. In later experiments, an iron-free starting composition (50Di50Le) was evaporated in helium or in hydrogen to determine the effect of the molecular weight of the furnace gas on the potassium isotopic fractionation of the evaporation residues. In all the one-bar experiments, the gas flow rates through the furnace tube were sufficiently slow (linear gas flow rate 24-70 cm/min) that the gas in the furnace tube would have had ample time to become saturated in the volatile species evaporating from the sample.

4.3 Analytical Procedures.

All evaporation residues were first analyzed for major element compositions using a JEOL JSM-5800LV SEM equipped with an Oxford Link ISIS-300 energy-dispersive microanalytical system. Concentrations of Na, Al, K, and Ca in the IIAB1 set of samples were also measured at Lawrence Livermore National Laboratory using a Thermo Electron XSeries quadrupole ICP-MS. A fully quantified analysis was performed using a linear calibration curve based on an in-house standard solution. An internal standard containing ^{6}Li, Sc and In was added to all standards and samples, and was used to correct for instrumental drift and signal suppression resulting from sample matrix effects. Samples were analyzed in a 2% HNO_3 matrix, at analyte concentrations within the range of concentrations used for the calibration. Serial dilutions of NIST certified reference materials were also analyzed, and used to evaluate accuracy of the analyses. The weight percents of Na_2O, K_2O, Al_2O_3, and CaO of the IIAB1 samples listed in Table 1 are those measured by ICP-MS. The internal precision of these measurements is in all cases better than 3.5% (2SD) of the reported value. With the exception of sample IIAB1-3, which had the lowest wt% K_2O, the wt% K_2O and the wt% Al_2O_3 measured by SEM are within ±8% of the concentrations measured by ICP-MS. The ICP-MS determined elemental abundances of the IIAB1 samples, including IIAB1-3, are taken to be more realistic values. The precision of the K_2O and Al_2O_3 measurements determine the precision with which we can estimate the fraction of potassium remaining in the evaporation residues, which in turn affects the estimate of the kinetic isotope fractionation factor of potassium by evaporation. The weight percent of K_2O and Na_2O of many of the samples (IIAB2-11 to IIAB2-29, IIAB5 samples and the 50Di50Le samples) were also remeasured using the University of Chicago electron probe (Cameca SX-50) with a rastered (~20 micron) beam. The weight percent K_2O and Na_2O listed for these

samples in Table 1 are those measured by electron probe. The weight percent K_2O and Na_2O of the IIAB2-1 to IIAB2-7 samples listed in Table 1 were measured only by SEM. For consistency with the other data in the table, the SEM measured concentrations were adjusted by a factor corresponding to the overall correlation between the SEM measured values and electron probe measured values from the set of samples for which both measurements were made. In every case, other than sample IIAB1-3, where we have compared two different types of concentration measurements, the results are linearly correlated with a scatter about the best fitting line of less than 10%. Because for present purposes we are mostly interested in concentrations relative to a starting composition, the linear correlation of the data obtained by different methods implies that we would come to much the same estimate regarding the amount of an element remaining in a given evaporation residue regardless of which set of concentration measurements are used. A precision of even 10% in the estimates of the elemental abundances of the evaporation residues does not significantly affect the estimate of the kinetic isotope fractionation factor of potassium.

The potassium isotopic composition of the evaporation residues was measured at the Lawrence Berkeley National Laboratory. Evaporation residues were dissolved for potassium isotopic analysis using a mixture of HF and HNO_3 in sealed Teflon vials on a hotplate. With dissolution accomplished, the solutions were dried down, re-dissolved in HNO_3, dried once again, and brought up in 300 μL of 1 M HNO_3 for loading on potassium separation columns. For chemical separation of potassium, a 1.8 ml bed of AG50x8 cation resin was used. Once the sample was loaded, the columns were eluted with 1 M HNO_3 and the potassium collected with 1 M HNO_3. Potassium isotopic measurements were carried out with a multiple-collector ICP source magnetic sector mass spectrometer (IsoProbe by GV Instruments). The IsoProbe features a RF only hexapole ion guide, in which various gases (e.g. He, H_2, Ne, Ar) can be dynamically introduced. In the case of the $^{41}K/^{39}K$ measurements reported here, Ne and H_2 were used in the hexapole to provide energy focusing as well as to remove Ar ion species. A positive potential was applied to the extraction lens to suppress secondary discharge and avoid memory effects from the skimmer and extraction cones. A static beam measurement was used with three of the nine available Faraday collectors set to simultaneously collect masses 39, 40, and 41 (Axial, H1, H2, respectively). Our measurement routine included peak blank subtraction from the measured ion beams. Twenty cycles of data were collected with an integration time of five seconds. Sample solutions were introduced to the IsoProbe using a desolvation nebulization system (Aridus II, Cetac Technologies) and a teflon nebulizer with a 60 μL/min uptake rate. Sample solutions were prepared from dried aliquots in 2% HNO_3 to match potassium concentrations of 400 ppb. Analysis runs of the experimental solutions were bracketed with runs of a solution of the source material (K_2CO_3) for the potassium in the starting compositions. Approximately 150 ng of potassium was used per isotopic analysis run. Reproducibility of the $^{41}K/^{39}K$ values was on the order of ±0.3‰ (2σ). We found no measurable isotopic fractionation of potassium when comparing the solution of the K_2CO_3 to the same solution passed through the column separation process.

Interpreting the results of the evaporation experiments in terms evaporation coefficients requires a thermodynamic model for the equilibrium vapor pressures of the volatile species over the starting material and evaporation residues. The thermodynamic model is also used to develop parameterizations of the evaporation rates of sodium and potassium as a function of melt composition, temperature, and oxygen fugacity of the surrounding gas. The thermodynamic model used in the present study was described in Ebel and Grossman, 2000).

5. EVAPORATION TRAJECTORIES

The evaporation trajectories of chondrule-like liquids evaporated under different conditions can provide a test of whether evaporation can explain the range of compositions observed for a given set of chondrules. If, for example, the experimental trajectories were found to be distinctly different from that defined by the chondrule sample set, volatility could be ruled out as having had a significant effect on the composition of that set of chondrules. These considerations were part of the motivation for carrying out a series of evaporation experiments with different starting compositions that were run under different conditions. These experiments also provide the key data on the evaporation kinetics and the isotopic fractionation associated with the evaporation of potassium.

Figure 8 shows the trajectory in composition space of K_2O-Na_2O and FeO-Na_2O in vacuum evaporation residues starting from the potassium-enriched composition IIAB1. The wt% of these oxides was normalized by dividing them by the wt% Al_2O_3, which is sufficiently refractory that it can be regarded as a conserved quantity under the conditions of the experiments. This normalization makes the evaporation trajectories reflect the true loss of the components, whereas changes in the weight percent will include effects due to the net weight loss of the residue.

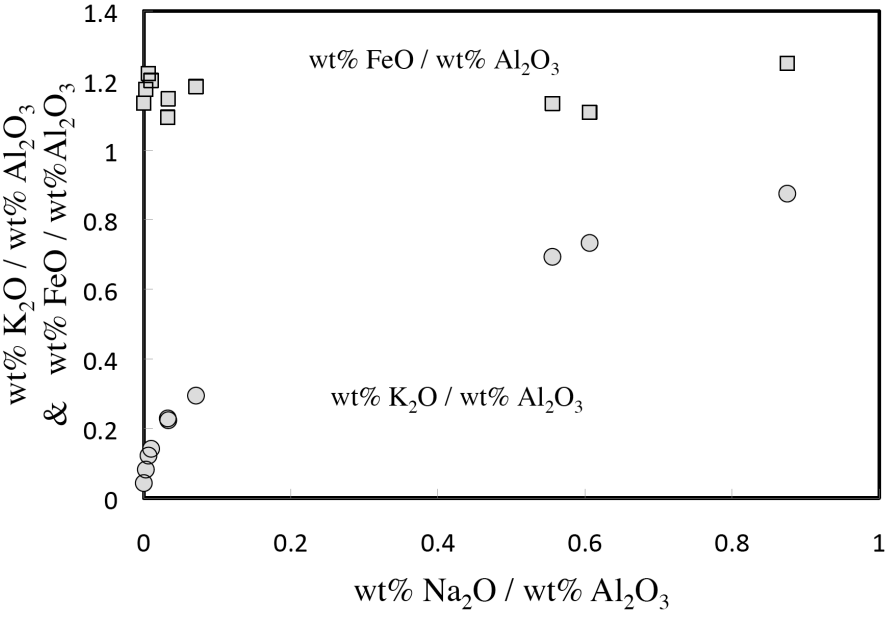

Figure 8. Composition of vacuum evaporation residues evaporated at a constant temperature T=1470˚C starting from the potassium-enriched composition IIAB1. The square symbols indicate the wt%FeO/wt%Al_2O_3 and the circles the wt%K_2O/wt%Al_2O_3 of the evaporation residues.

The trajectory in wt% K_2O versus wt% Na_2O shown in Fig. 8 is similar to what one can construct from the data reported by Yu et al., (2003). Figure 8 shows that under vacuum evaporation conditions there is no resolvable loss of FeO while sodium or potassium are still present in the residue. Figure 9 shows that when a chondrule-like composition is evaporated in a one-bar stream of gas at T~1430˚C and log$f$$O_2$=IW+2.5 iron becomes sufficiently volatile that a measurable fraction evaporates while sodium and potassium are still present. This result is not unexpected in that the evaporation rate of FeO will increase, in more reducing conditions, in proportion to $f{O_2}^{-1/2}$ whereas the evaporation rate of K_2O and Na_2O will increase only as $f{O_2}^{-1/4}$ (see discussion in Richter et al. 2002).

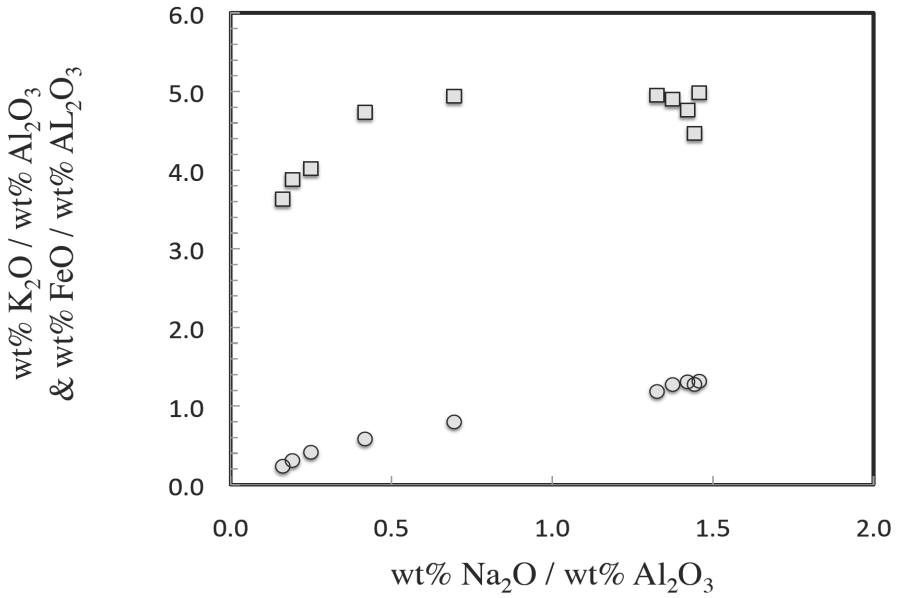

Figure 9. Oxide ratio trajectories of IIAB5 residues evaporated at T~1430˚C into a one-bar flowing stream of H_2+CO_2 gas with log$f$$O_2$=IW+2.5. The square symbols indicate the wt%FeO/wt%Al_2O_3 and the circles the wt%K_2O/wt%Al_2O_3 of the evaporation residues.

The IIAB1 and IIAB5 compositions used to determine the evaporation trajectories in Figs. 8 and 9 were significantly enriched in the K_2O component compared to natural Type IIA chondrules for there to be sufficient potassium left in the more highly evaporated samples for reasonably precise potassium isotopic analyses. Because of this, the trajectories and associated evaporation rate of potassium are not directly applicable for interpreting actual chondrule data. Figure 10 shows both vacuum and one-bar evaporation trajectories from a starting composition with the wt% of K_2O about one tenth

that of Na_2O, which is the typical ratio in olivine-rich chondrules. For these low-potassium starting compositions the trajectories of the vacuum evaporation residues and those from the one-bar experiments are not significantly different once one takes into account the somewhat different sodium and potassium contents in the starting compositions.

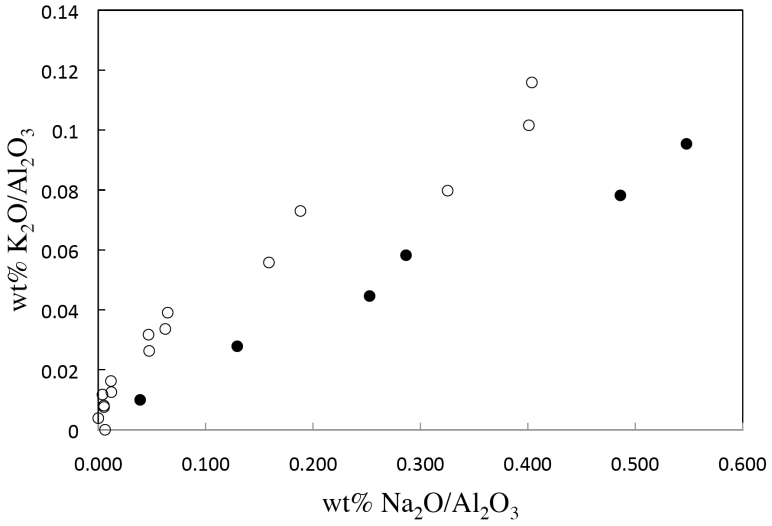

Figure 10. Composition of evaporation residues run at T=1470˚C in vacuum (open circles) and at T=1430˚C in one bar H_2+CO_2 gas with log fO_2=IW+2.5 (black circles).

6. EVAPORATION KINETICS

The residues used to make the plots of the evaporation trajectories given in the preceding section also provide data regarding the evaporation kinetics of sodium and potassium from chondrule-like liquids. Figure 11 shows the average evaporation rate in moles per cm^2 per second of residues evaporated in vacuum for different lengths of time at T=1470˚C and different starting compositions. The figure shows the effect of concentration on the evaporation rate, most obviously in the case of potassium where the evaporation rate of the low potassium starting composition samples are much less than that those of the higher potassium starting composition. Because of such compositional effects, as well as the effects of temperature and oxygen fugacity, the more general way of reporting evaporation kinetics is in terms of evaporation coefficients defined in Eqn. (1). In the specific case of vacuum evaporations (i.e., $P_i = 0$) the resulting equation for calculating the evaporation coefficients is simply

$$\gamma_i = (J_i / P_i^{sat})\sqrt{2\pi m_i RT} \qquad (8)$$

Thus, to determine evaporation coefficients the evaporation rates J_i have to be combined with a thermodynamic model to determine the mass m_i and saturation vapor pressure P_i^{sat} of the dominant gas species in equilibrium with the condensed phase. Equation (8) is used for determining the evaporation coefficient of sodium and potassium from a chondrule-like melt given that the dominant gas species are Na and K and that the

saturation vapor pressure of other molecules, such as KO or NaO, are negligible by comparison. One complication in applying Eqn. (8) is that the evaporation rates measured in our experiments are averages over some finite time during which the composition of the condensed phase changes. There are various ways to deal with this. One can extrapolate the measured evaporation rates shown in Fig. 11 to zero time and use this in connection with the saturation vapor pressure over the starting composition. This is problematic in the case of highly volatile species such as sodium and potassium in that a significant amount of evaporation will have taken place while the sample was being brought to the final run temperature and thus the measured evaporation rate does not correspond to a specific temperature.

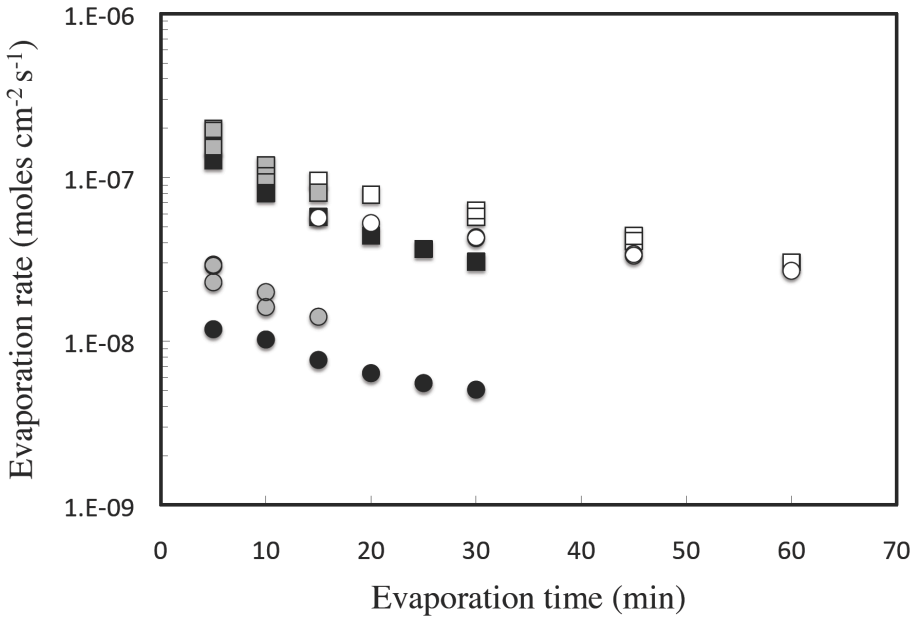

Figure 11. Na and K vacuum evaporation rates in moles per cm^2 per second as a function of run duration for the potassium-rich starting composition IIAB1 (Na, open square; K, open circles), for residues IIAB2-1 to IIAB2-7 (Na, black squares; K, black circles), and for vacuum residues with sample numbers between IIAB2-11 to IIAB2-29 (Na, gray squares; K, gray circles). The evaporation rates shown represent the average rate for the duration of each experiment. The relatively small differences between the Na evaporation rates from the IIAB1 and IIAB2 samples compositions is due to there being more Na in the IIAB1 starting composition (2.25 wt%) than in IIAB2 (~1 wt%). The much larger difference in the evaporation rate of potassium between the various sets of samples reflect the potassium concentration in the zero-time runs that are used as the effective starting composition for calculating the evaporation rates.

The approach we use to determine γ_i involves first calculating a vacuum evaporation trajectory from the zero-time composition to that of a given residue assuming the evaporation coefficient is equal to one. The calculation also takes into account the changing surface area and the changing saturation vapor pressures as the composition evolves. The vapor pressures for sodium and potassium are calculated using the thermodynamic model described in Ebel and Grossman (2000). Even though the

calculation applies to the vacuum limit when there is no gas surrounding the sample, the vapor pressures that are relevant for calculating the evaporation coefficients are those that would result if the evaporating species had been allowed to reach equilibrium with the melt. The actual evaporation coefficient of a given residue is given by the ratio of the calculated time to reach that particular residue composition divided by the duration of the experiment that produced the residue. The evaporation time calculated assuming $\gamma = 1$ is typically about an order of magnitude shorter than the duration of an actual experiment indicating that $\gamma_i \sim 0.1$. Comparing the evaporation coefficients determined in this way for residues run for different lengths of time from a common starting composition provide an estimate of the internal consistency of the evaporation coefficients reported in Table 2 as composition-independent quantities. The nominal precision of the evaporation coefficients listed in Table 2 corresponds to one standard deviation reflecting the range of estimates derived from a set of evaporation residues from a particular starting composition held at high temperature for different amounts of time. Also shown in Table 2 are the evaporation coefficients reported by Fedkin et al. (2006) based on their analysis of evaporation residues from experiments reported by Yu et al. (2003) and those reported by Alexander (2002) derived by applying his EQR thermodynamic model to data given by Yu and Hewins (1997). The agreement between our data and the earlier reports of the evaporation coefficients are reasonable when one compares our vacuum results with the evaporation coefficients derived from the Yu et al. (2003) and Yu and Hewins (1997) residues that were run in air at 10^{-5} bars. The range of values derived from our experiments reflect real uncertainties not only in the chemical composition of the starting and final composition, but also the surface areas of the samples that are hard to measure precisely and change during the course of an experiment. Fedkin et al. (2006) also reported evaporation coefficients for some of the residues that Yu et al. (2003) evaporated in low-pressure hydrogen, but these are about an order of magnitude smaller than those for the same composition evaporated into 10^{-5} bars air. There are a number of reasons we believe that this claimed large effect of hydrogen on the evaporation coefficients should be treated with some skepticism. To begin with, Richter et al. (2002) found no such effect on the evaporation coefficients of silicon and magnesium evaporating from a CAI-like liquid into vacuum compared to evaporations into hydrogen at 10^{-4} bars, which at the very least raises the question of why the alkalis should be so different in their sensitivity to the surrounding gas. Furthermore, as we discuss below, there is isotopic evidence suggesting that the Yu et al. (2003) hydrogen evaporation residues were significantly affected by recondensation, which would result in low net evaporation, and thus a calculation such as that by Fedkin et al. (2006) would determine too small an evaporation coefficient. Another potential experimental problem with evaporation into hydrogen is that one has to take great care to ensure that the room-temperature hydrogen flowing in a low-pressure furnace has sufficient collisions to achieve the equilibrium speciation of H relative H_2. The lack of equilibrium speciation of hydrogen can easily lower the evaporation rates by as much as an order of magnitude. An example of this can be seen by comparing evaporation rates reported by Kuroda and Hashimoto (2002), who took special care to reach thermal and hydrogen speciation equilibrium in their low-pressure hydrogen furnace, with the order of magnitude lower evaporation rates reported by Nagahara and Ozawa (1996) for experiments at the same temperature and hydrogen pressure in a furnace very much like that used by Yu et al.

(2003). It seems quite possible that the low values of the evaporation coefficients estimated by Fedkin et al. (2006) for evaporation into hydrogen reflect artificially low evaporation rates rather than a significant effect of hydrogen on the evaporation coefficients.

7. ISOTOPIC FRACTIONATION OF EVAPORATION RESIDUES

In this section we consider the relationship between the amount of an element volatilized and the associated isotopic fractionation of the evaporation residue. Two types of experiments were used for this purpose. One set involved evaporation into vacuum and a second set involved evaporations into a slowly flowing stream of one-bar gas of various compositions. Our expectation in designing these two types of experiments was that the vacuum experiments would determine the isotopic fractionations in the purely kinetic evaporation regime as given by Eqn. (4), while the isotopic fractionation of residues from the one-bar experiments would yield an estimate or bound on the equilibrium isotope fractionation between silicate liquid and surrounding gas. As shown below, we were correct in our expectations regarding the vacuum experiment results, but quite wrong regarding the isotopic composition of residues from the one-bar evaporation experiments.

7.1 Isotope Fractionation by Evaporation into Vacuum

The potassium isotopic composition of evaporation residues from the IIAB-1 set of experiments are plotted in Fig. 12 as $1000 \times \ln\left(\frac{(^{41}K/^{39}K)residue}{(^{41}K/^{39}K)start\ comp.}\right)$ versus $-\ln f_{^{39}K}$, where $f_{^{39}K}$ is the fraction of the initial ^{39}K remaining in the residue. When isotope data are plotted in this way, fractionations following a Rayleigh fractionation law (Eqn. 5) will fall on a line with slope equal to $1000(1-\alpha_K)$ where α_K is the kinetic isotope fractionation between the evaporation flux and the condensed phase. Also plotted in Fig. 12 is the isotopic composition of residues from the four lowest pressure experiments reported by Yu et al. (2003). Yu et al. (2003) only report the ratio of the weight percent of potassium in their evaporation residues to that in the starting composition (i.e., their quantity K/K_o), which due to both isotopic fractionation and evaporation of species besides potassium (i.e., sodium) is not exactly the same as the fraction of ^{39}K remaining. However the difference is small (~5%), thus when we plot the Yu et al. (2003) data in Fig. 12 we use their reported K/K_o for $f_{^{39}K}$.

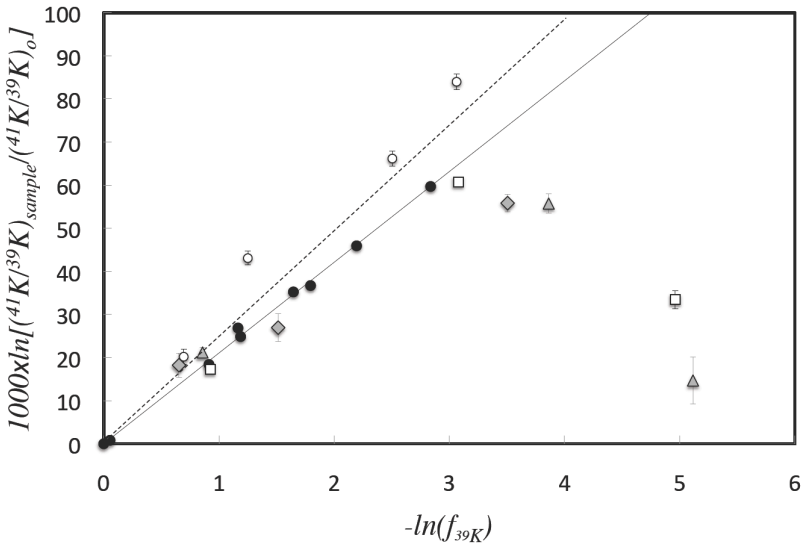

Figure 12. Potassium isotopic fractionation of evaporation residues versus f_{39K}, the fraction of ^{39}K remaining in the residue, plotted in a manner such that Rayleigh fractionation with a constant kinetic isotope fractionation factor α_K would result in the data falling on a line with slope 1000(1-α_K). The black circles correspond to vacuum evaporation residues from the present study (2s error bars are smaller than the symbols). The zero-time run sample ABII1-9 is used as the effective starting composition and the potassium isotopic compositions plotted are relative to that of this sample. All other data points are from Yu et al., 2003 (P=1×10^{-5} air as open circles, P=1.8×10^{-5} air as open squares, P=7.1×10^{-5} H_2 as grey triangles, P=9×10^{-5} H_2 as grey diamonds). The error bars for these are taken from a quantity listed as *err* in Tables 2a and 2b of Yu et al. (2003), which is not defined in the text but appears to correspond to one standard deviation of repeated analyses of the sample. The dashed line corresponds to Rayleigh fractionation of $^{41}K/^{39}K$ with $\alpha_K = (39/41)^{1/2}$ while the solid line is the best fitting line to our vacuum data and has a slope corresponding to $\alpha_K = (39/41)^{0.43}$.

There are various things worth noting regarding the data plotted in Fig. 12. To begin with, our data fall very nearly on a line, as expected for Rayleigh fractionation, with a slope corresponding to α_K = 0.9790±0.0015 at the 95% confidence level. This value of α_K corresponds to $(39/41)^{\beta}$ with β=0.43±0.03. It has often been assumed that kinetic isotope fractionations should be governed by a fractionation factor equal to the inverse square root of the evaporating species (i.e., β=0.5), which for potassium would produce residues with isotopic compositions falling along the dashed line in Fig. 12. All previous studies of kinetic isotope fractionations by vacuum (P<10^{-6} Torr) evaporation of silicate liquids found these to correspond to Rayleigh fractionation with the exponent β always less than 0.5 (Davis et al., 2000; Wang et al., 2001; Richter et al., 2002, 2007; Dauphas et al., 2004; Knight et al., 2009). Our finding β for potassium to be somewhat less than 0.5 is thus not surprising. The Yu et al. (2003) potassium isotopic data either do not follow a Rayleigh fractionation law, or in the one case when they do more or less fall along a line (the P=10^{-5} bar air experiments) the slope is such that β>0.5, which is hard to understand. All their other experiments do not follow a Rayleigh fractionation

behavior, which they suggested was due to recondensation. This seems a reasonable explanation, and as noted earlier, recondensation will result in underestimates of the true free evaporation rate of potassium or sodium. Based on the goodness of the fit of our data to a Rayleigh fractionation law and similar values of $\beta<0.5$ for all other silicate evaporation residues produced in the same vacuum furnace used here (Davis et al., 2000; Wang et al., 2001; Richter et al., 2002, 2007; Dauphas et al., 2004; Knight et al., 2009), we believe it is reasonable to adopt $\beta=0.43\pm0.03$ as a realistic value for calculating the free-evaporation fractionation factor of potassium isotopes evaporating in the vacuum limit (i.e. $P_k / P_{k,sat} << 1$). Several earlier studies of magnesium and silicon isotopic fractionation by evaporation (Richter et al., 2002, 2008 and Knight, 2009) showed that while the kinetic isotope fractionation factor can depend on temperature, as is the case for magnesium, it does not seem to be significantly different for evaporation into vacuum or into a low-pressure hydrogen-dominated gas. Until potassium evaporation experiments are run in low pressure thermally-equilibrated gases with the equilibrium speciation of H and H_2, and no significant recondensation, we suggest that a kinetic isotope fractionation factor for potassium calculated using $\beta=0.43$ is the present best estimate for both vacuum and low pressure conditions.

7.2 Isotope Fractionation by Evaporation into a Flowing Gas.

The motivation for the experiments done in a gas-mixing vertical tube furnace where molten chondrule-like compositions were exposed to a slowly flowing gas was to explore conditions such that evaporation could deplete the melt of its more volatile components without significant isotopic fractionation. The typical flow rate of the gas introduced to the furnace was about 250-550 cm^3/minute at room temperature and 1 bar pressure. The inner volume of the furnace tube is about 500 cm^3, thus the residence time of gas in the furnace tube, τ_{res}, is about 30 seconds to one minute. The timescale for the evaporating potassium to saturate the furnace gas, τ_{sat}, is given by the ratio of the moles of potassium required to saturate the gas in the tube furnace divided by the evaporation flux. This saturation timescale is of the order of a second (see Appendix), which being much less that the residence time of gas in the furnace tube means that the one-bar experiments involve evaporation and fractionation in the equilibrium limit. As saturated gas is continuously being removed from the system, the volatile-free gas being introduced into the furnace to replace it has to become saturated in volatiles by evaporation from the molten sample. The melt will thus become progressively depleted in elements in proportion to their relative saturation vapor pressures. We had expected the associated isotopic fractionation of the evaporation residues to be negligible because at the high temperature of the experiments the equilibrium isotopic fractionation between silicate and vapor should be extremely small. We had hoped that these experiments would be a very straightforward demonstration of conditions where elements can be fractionated by evaporation from a silicate liquid without measurable isotopic fractionation. Figure 13 shows that contrary to our expectation measurable isotopic fractionations were still present in the residues evaporated into one-bar of slowly flowing gas even though $\tau_{sat} << \tau_{res}$.

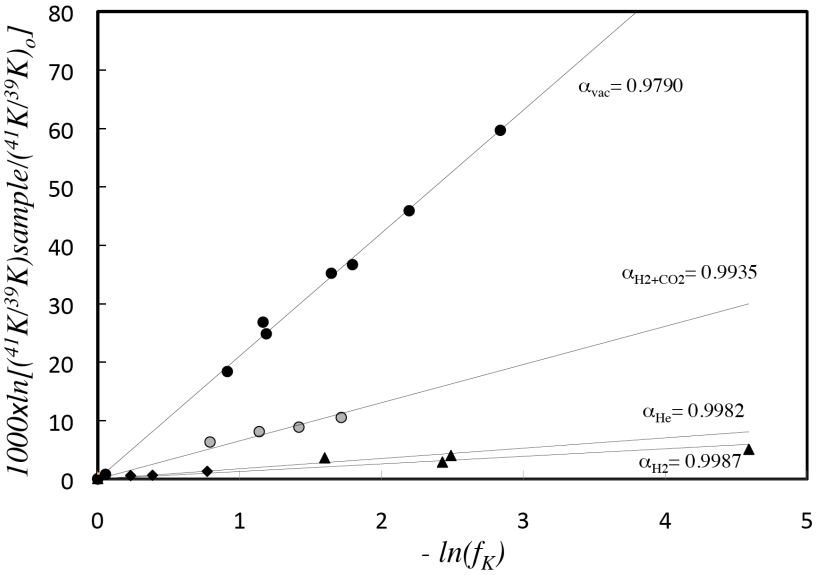

Figure 13. Potassium isotopic fractionation of evaporation residues versus the fraction of ^{39}K remaining in the residue plotted in a manner such that Rayleigh fractionation with a constant kinetic isotope fractionation factor α_K would result in the data falling on a line with slope 1000(1-α_K). Residues evaporated into vacuum are shown as black circles, while residues evaporated in one bar of slowly flowing CO_2+H_2 (logfO_2=IW+2.5) are shown as gray filled circles, in He as black diamonds, and in H_2 as black triangles. The values shown for the kinetic isotope fractionation factors α for the various sample sets are derived from the best fitting line through the data points from each separate set of experiments.

The first set of one-bar evaporation experiments were run in a mixture of about 70%CO_2+30%H_2 to maintain the fO_2 close to the iron-wüstite equilibrium value, which is reasonable for chondrules such as those from Semarkona that have coexisting iron metal and iron oxide. The results of this first set of one-bar experiments showed surprisingly large potassium isotopic fractionations despite the molten silicate and its surrounding vapor having had ample time to equilibrate. Given the high temperature and low flow rate of these experiments it seems very unlikely that these large isotopic fractionations are due to equilibrium isotopic fractionation of potassium between melt and vapor. What we had not taken into account in designing the one-bar experiments was the effect of a large temperature gradient in the furnace between where the molten sample was placed (T~1430˚C) and the ends of the furnace tube where water-cooled fittings are used to maintain gas-tight seals. Because the gas in the furnace will locally be close to equilibrium and saturated in the volatile species, there will be a gradient in the potassium vapor pressure associated with the temperature gradient. The transport of potassium away from the evaporating sample will then be due at least in part to diffusion of potassium in the gas. A derivation and estimate of the relative importance of the advection by the flowing gas and diffusion is given in the Appendix showing that they are more or less equally important in transporting potassium away from the vicinity of the evaporation sample. A key point is that the diffusive part of the transport of potassium in the furnace

gas will fractionate isotopes because of the greater mobility of the lighter isotopes. The mobility, or equivalently the diffusion coefficient, of a dilute gas species of mass m_i in a bulk gas of mean molecular weight M is proportional to the square root of the reduced mass $\mu_{i,M} = \frac{m_i M}{m_i + M}$. The CO_2+ H_2 gas mixture in the furnace has a mean atomic weight of about 30. The kinetic fractionation factor for diffusion, α_{diff}, of ^{41}K from ^{39}K in this gas is then the ratio of the square root of the respective mobilities, $\alpha_{diff} = \sqrt{\frac{\mu_{39,30}}{\mu_{41,30}}} = 0.9893$. The measured value of the kinetic isotope fractionation factor for potassium in the one-bar CO_2+ H_2 evaporation experiments is 0.9935, which is consistent with about 50% of the transport of potassium away from the molten sample being by diffusion.

The evaporation experiments into one-bar of helium or hydrogen provide a test of the idea that diffusion in the furnace gas was responsible for the isotopic fractionation of potassium in the one-bar experiment residues. Because of the effect of the mean molecular weight of the dominant gas in the furnace on the reduced mass of the potassium isotopes, the theoretical diffusive fractionation factors become $\alpha_{diff} = 0.9977$ in helium and $\alpha_{diff} = 0.9988$ in hydrogen. The very much smaller measured values of the potassium isotope fractionation of residues evaporated into helium or hydrogen (α = 0.9982 and 0.9987) compared to those evaporated into the CO_2+ H_2 gas is exactly what is expected if the fractionation is due to diffusion in the dominant furnace gas. The fact that the fractionations in helium and in hydrogen are quite similar despite the fact that the evaporation rate is about an order of magnitude faster in hydrogen than in helium confirms that the assumption of local equilibrium is met. The fact that the fractionations in the helium and in the hydrogen experiments are closer to the pure diffusive limit than in the case of the CO_2+ H_2 experiments is also expected in that potassium diffuses considerably faster in helium or hydrogen than in the CO_2+ H_2 gas, and thus the Peclet number is significantly smaller (i.e., more diffusive transport relative to advection) with helium or hydrogen as the dominant furnace gas.

Figure 13 illustrates conditions where significant amounts of potassium can be evaporated with very different degrees of associated isotopic fractionation of the potassium remaining in the residue. Clearly, the lack of significant isotopic fractionation of a silicate material does not preclude this material having lost a significant fraction of its more volatile components by evaporation.

8. DIFFUSIVITY OF POTASSIUM IN CHONDRULE-LIKE MELT

The degree to which evaporation of a volatile species from a molten chondrule is diffusion limited depends on the ratio of the time it would take for diffusion to homogenize the distribution of component *i* divided by the time it would take evaporation to remove *i*. The quantity that still needs to be determined in order to evaluate the possibility of potassium being diffusion-limited when evaporating from a chondrule-like liquid is the diffusion coefficient of potassium in the melt.

A series chemical diffusion experiments were run to measure the diffusion of potassium in a chondrule-like melt. The diffusion couples were made by juxtaposing potassium-enriched (4.8 wt% K_2O) and potassium-poor (0.3 wt% K_2O) powders of otherwise chondrule-like composition. The couples were then annealed for times ranging from thirty minutes to four minutes in a piston cylinder assembly run at 1650˚C and 1.1 GPa. (see Richter et al., 2003 for a detailed description of diffusion experiments using similar assemblies). The results were surprising in that, as shown in Fig. 14, even in the four-minute experiment the potassium composition had evolved to a weak liner gradient that is almost certainly a steady state Soret diffusion profile due to a small temperature difference across the diffusion couple (see Richter et al., 2009b for examples of piston cylinder Soret diffusion experiments). The fact that the same linear profile was seen in diffusion couples run for thirty minutes, ten minutes, and four minutes is the evidence that the profiles had all reached a steady state. In order for a 4.5 mm long sample run for four minutes at 1650˚C to have equilibrated requires $D_K > 2\times10^{-4}$ cm^2/s.

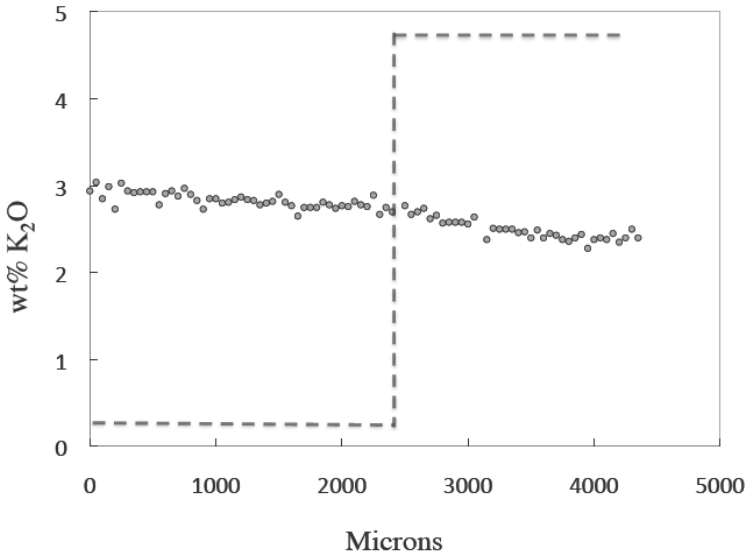

Figure 14. Potassium concentration measured along the long axis of a diffusion couple annealed for four minutes at 1650˚C and 1.1 GPa in a piston cylinder assembly. The dashed line shows the initial step in concentration and the small filled circles are the wt% K_2O measured along the long axis of the sample using a SEM equipped with an Oxford Link ISIS-300 energy-dispersive microanalytical system. The measured compositions fall along a weakly sloping line that is interpreted to be a steady state Soret diffusion profile due to a small temperature gradient across the sample while at the nominal run temperature of 1650˚C.

9. SUMMARY AND DISCUSSION

The olivine-rich Type IIA and Type IA chondrules from Semarkona have textures showing that they must have been melted to a high degree, which depending on the bulk composition requires temperatures in the range 1550˚C to 1750˚C (see Table 1 in Alexander et al., 2008). Textural studies have been used to infer cooling rates from above or near liquidus temperatures in the range 5-1000K/hr (see Table 1 in Desch and Connelly, 2002). Despite having been molten, the Type IIA chondrules from Semarkona show no evidence of volatilization of sodium and potassium, if anything, they appear to be slightly enriched in these two elements relative to much more refractory aluminum (Figs. 1 and 4). In contrast to this, the Type IA chondrules from Semarkona are significantly depleted in sodium and potassium relative to aluminum when compared to the solar abundance ratio of these elements (Figs. 1 and 6), which could be evidence of volatilization during melting or simply a property of the precursor that was later melted. However, neither the Type IIA nor the Type IA chondrules from Semarkona have systematic isotope fractionations of potassium (Fig. 7) of the sort that characterize kinetic isotope fractionation of volatile components evaporating from a molten silicate into a low pressure environment (Fig. 13).

The chemical properties of the Type IA and Type IIA Semarkona chondrules raise a number of questions regarding the conditions such that melting did not produce any obvious loss of alkalis from the Type IIA chondrules and no significant or systematic isotopic fractionation of potassium of either type of chondrules. The simplest explanation for the lack of isotopic fractionation one might consider is that the duration of partial melting was simply too short to allow for any significant evaporation of sodium or potassium. This idea can be tested using the experimental data on the evaporation rate of alkalis from chondrule-like liquids (Section 6) taking into account the effect of temperature and oxygen fugacity on the saturation vapor pressure. Combining the measured vacuum evaporation rate of potassium at T=1743 K from a sample with 0.3 wt% K_2O (see Fig. 11) with thermodynamic calculations for the fO_2 that is relevant to the vacuum experiments (i.e., $fO_2=1.7\times10^{-6}$ bars, which is the oxygen fugacity that would be in equilibrium with the melt if all the gas species were derived from the melt) and the saturation vapor pressure as a function of concentration, temperature (activation energy ~ 600 kJ), and oxygen fugacity (increasing in proportion to $fO_2^{-1/4}$) results in a parameterization of the evaporation rate of potassium (moles/cm^2 s) as

$$J_K \sim 7.0\times10^{-8}\, C_K\, (1.7\times10^{-6}/fO_2)^{1/4}\, e^{-(E_K/RTo)(To/T-1)} \qquad (9)$$

where C_K is wt% K_2O in the melt, T_o (=1743K) is the reference temperature, E_K is the activation energy (600 kJ), and R is the gas constant. Figure 15 shows the cooling rates as a function of fO_2 and peak temperature that would result in a 40% loss of the original potassium by evaporation from a molten chondrule with an initial radius of 1 mm. The calculations used to construct Fig. 15 are based on Eqn. (9) for the evaporation flux and thus represent the limiting case of free evaporation (i.e., no recondensation), which would result in an isotopic fractionation of the residue of $\delta^{41}K \sim 10‰$. The log fO_2 corresponding to the iron-wüstite equilibrium (IW) at the various temperatures is also shown. The Semarkona chondrules typically have both iron metal and iron oxides, thus the oxygen fugacity must have been close IW. Figure 15 thus shows that if the

Semarkona chondrules while molten (T>1743K) were surrounded by a gas with fO_2 close to IW, cooling rates significantly greater than those inferred from chondrule textures would have been required for there not to have been significant evaporation of potassium and associated large isotopic fractionations. Given the weak dependence of the evaporation rate on fO_2, the basic argument illustrated by Fig. 15 would hold even if the actual fO_2 had been several log units larger or smaller that IW. The conclusion to be drawn from Fig. 15 is that the relatively limited isotopic fractionation of the Semarkona chondrules (Fig. 7) cannot be explained by the high temperature event that melted the chondrules having been too short for significant free evaporation of potassium.

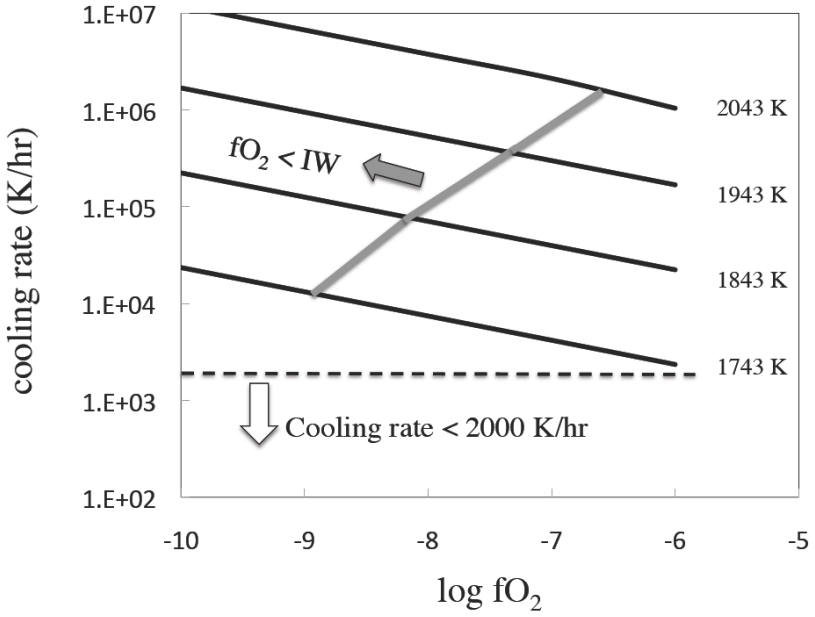

Figure 15. The four black lines show calculated cooling rates from the indicated peak temperature as a function of fO_2 that would result in 40% loss of the original potassium from a one millimeter radius chondrule with an initial 0.2 wt% of K_2O. This amount of free evaporation of potassium would result in a residue enriched in $^{41}K/^{39}K$ by about 10‰. The heavy gray line joins points on the peak temperature lines where the fO_2 is that of the iron-wüstite equilibrium.

Galy et al. (2000) argued for there having been a high surrounding gas pressure, perhaps as large as one bar, while chondrules were molten and that this would have affected their isotopic fractionation. Our one-bar evaporation experiments showed that isotopic fractionation is not eliminated by a high surround pressure of gas, but rather that the fractionation persists due to isotopic fractionation as the evaporated species diffuse through the surrounding gas. Richter et al. (2002) has already shown that this gas phase fractionation becomes important for evaporation into an effectively infinite surrounding gas once the pressure exceeds about 10^{-3} bars. Once the surrounding pressure reaches one bar, the isotopic fractionation is entirely due to diffusion in the gas and the fractionation factor becomes the inverse square root of the reduced mass of the isotopes (see Eqn. 7 and associated discussion). As was illustrated by Fig. 13, the degree of isotope fractionation by transport in the surrounding gas will still be large for a gas with an oxygen fugacity that is close to that of the iron-wüstite, but small in a hydrogen-

dominated gas. Given the evidence that the Semarkona chondrules evolved in a gas with fO_2 close to IW, a high surrounding gas pressure would have produced potassium isotopic fractionations in evaporation residues much larger than what has been reported.

Both Young (2000) and Galy et al. (2000) have suggested that a possible reason why chondrules show so little isotopic fractionation is that they were in a diffusion-limited evaporation regime. The nondimensional parameter they used to measure the degree to which evaporation would be limited by diffusion in the silicate liquid is a Peclet number, which they defined as $Pe = \frac{r\,dr/dt}{D}$ where r is the radius of the molten materials (assumed to be a sphere) dr/dt is the retreat velocity of the surface due to evaporation, and D is the diffusion coefficient of the species of interest in the silicate liquid. These papers argued that a large constant Peclet number (>100) would effectively suppress the isotopic fractionation of an evaporation residue. In the case of the Semarkona chondrules, the major evaporating component of the liquid is Na_2O, thus we can use the evaporation rate of sodium to estimate a realistic value for the relevant Peclet number. The evaporation rate J_{Na} of sodium (moles/cm^2 per second) as a function of temperature and oxygen fugacity can be parameterized as

$$J_{Na} \sim 1.0\times10^{-7}\, C_{Na}\, (1.0\times10^{-6}/fO_2)^{1/4}\, e^{-(E_{Na}/RTo)(To/T-1)} \qquad (10)$$

where C_{Na} is the wt% Na_2O in the melt, E_{Na} is the activation energy (~500 kJ), T_o (= 1743K) is the reference temperature, and R is the gas constant. The molar flux of Na_2O, $J_{Na_2O} = J_{Na}/2 \sim 1\times10^{-5}$ moles/cm^{2}s for T=1943 K and fO_2 corresponding to the iron-wüstite equilibrium. The rate of volume change due to the evaporation of the Na_2O component is $dV/dt = J_{Na_2O} A \nu$ where A is the surface area and ν is the molar volume of the Na_2O in the liquid. For a spherical chondrule of radius r, $dV/dt = A\,dr/dt$, thus $dr/dt = J_{Na_2O}\,\nu$. The Peclet number for a 1 mm diameter chondrule at 1943K and fO_2 of IW is then $Pe = rJ_{Na2O}\nu/D_{Na}$ which for ν~20 cm^3/mole and $D_{Na} \sim D_K > 2\times10^{-4}$ cm^2/s gives $Pe <$ 0.1. This estimate of the Peclet number is many orders of magnitude too small to explain the lack of isotopic fractionation of chondrules during evaporation in the manner proposed by Young (2000) and Galy et al. (2000). The reason that the Peclet number is so small is that dr/dt is small because of the low concentration of the major evaporating component (Na_2O) and its fast diffusion in chondrule-like liquids. But the larger point is that using a Peclet number based on the retreat velocity *(i.e.,* $Pe = \frac{r\,dr/dt}{D}$) is not the right way to characterize the potential for diffusion-limited evaporation when only minor components of the bulk composition are volatilized.

Richter et al. (2002) used a component-specific characterization of diffusion-limited evaporation to show that isotopic fractionation can be suppressed even in the limit of very small overall Peclet number. Diffusion-limited evaporation will result regardless of the magnitude of dr/dt whenever the time it takes to evaporate a given component τ_{evap} is fast compared to the time τ_{diff} required for diffusion to maintain the homogeneity of the evaporated residue. The ratio of these timescales for a component *i*

define a component-specific evaporation number $E_{vi}=3J_i r/\rho_i D_i$ (see Richter at al. 2002 for derivation and discussion), where J_i is the evaporation flux of i, r is the radius, ρ_i is the molar density of component i, and D_i is the diffusion coefficient. Richter et al. (2002) used model calculations to show that in the case of magnesium evaporating from a CAI-like liquid the isotopic fractionation was suppressed by a factor $E_{vMg}^{-0.09}$ relative to the free evaporation isotopic fractionation. The potassium isotopic fractionation of a chondrule-like evaporation residue will be similarly affected by E_{vK}. The magnitude of the potassium evaporation number for a Type IIA Semarkona chondrules with $\rho_{K_2O}=10^{-4}$ moles/cm^3 (see Fig. 2 and 3 for typical concentrations), $D_K>2\times10^{-4}$ cm^2/s, and $J_{K_2O} = J_K/2 \sim 1.5\times10^{-6}$ moles/cm^{2}s (calculated using Eqn. 9 for T=1943 K and fO$_2$=IW) will be $E_{vK} \sim 200r$ where r is the radius measured in centimeters. By this estimate the evaporation number for potassium evaporating from a 1 millimeter diameter Type IIA-like chondrule will be about 10. The potassium evaporation number for the Type IA chondrules of the same size will be similar because the lower molar density of potassium (see Fig. 5 for typical K_2O concentrations in Type IA chondrules) will be offset by a comparable reduction in the evaporation rate. Combining an evaporation number of 10 for potassium evaporating from a chondrule-like liquid with the parameterization $\delta^{41}K_{(Ev)} = \delta^{41}K_{(Ev=0)}e^{-0.09Ev}$ given by Richter et al. (2002) for the reduction of the isotope fractionation as a function of the evaporation number shows that the isotopic fractionation would be reduced by about 50%. This discussion of diffusion-limited evaporation of chondrules should be regarded as suggestive rather than quantitative in that the actual effect will vary depending on chondrule size, the specific temperature and fO$_2$ during evaporation. and the diffusion coefficient of potassium that might be somewhat larger than the lower bound on the diffusivity derived from our shortest duration diffusion experiment. The overall point is that diffusion-limited evaporation might have had some effect at reducing but not suppressing potassium isotope fractionation from molten chondrules.

Up to this point, we have shown that present estimates of the duration of the melting event affecting the Type IA and Type IIA chondrules are sufficiently long that significant amounts of potassium would have evaporated. We also showed that if the chondrules had evaporated into very dense surrounding gas, the residues would still have been fractionated by diffusion in the gas transporting the volatile species away from the evaporating surface. Thus, a high surrounding pressure would not explain the lack of isotopic fractionation associated with potassium evaporation. Under the right circumstances diffusion-limited evaporation could have reduce the isotopic fractionation of a melt containing a volatile species like potassium, but it does not seem likely that this could eliminate the isotopic fractionation entirely. Even in the limit of extreme diffusion-limited evaporation, one would expect that there would be significant isotopic fractionation due to the relative mobility of isotopes as they diffuse from the interior to the evaporating surface. Our preferred explanation as to why the Semarkona chondrules retained significant amounts of highly volatile components and isotopically unfractionated potassium despite having been molten is that they reached equilibrium with a high-temperature surrounding gas before the potassium was entirely evaporated. Our one-bar evaporation experiments showed that evaporation into a slowly flowing effectively saturated gas will result in elemental fractionation that is proportional to the

flow rate times the saturation vapor pressure of the elements, and that the associated isotopic fractionation can be either large or small depending on the molecular weight of the surrounding gas and the relative importance of transport in the gas by advection and diffusion.

The general idea that chondrules did not become isotopically fractionated despite having been molten because they saturated their immediate environment was suggested by Alexander et al. (2000) and further discussed by Richter (2004) and Alexander and Grossman (2005). A number of questions arise in connection with an equilibrium explanation for the concentration and isotopic composition of potassium in Type IA and Type IIA chondrules from Semarkona. To begin with, how would such equilibrium be achieved? It would require that the partial evaporation of sodium and potassium be sufficient for their concentration in the surrounding gas to reach the saturation vapor pressure, which will depend on the volume density of chondrules that would be required. The saturation vapor pressure of potassium over a model molten Type IA chondrule (0.03 wt% K_2O, T=1943 K, and fO_2 corresponding to IW-1.5) calculated as described in Ebel and Grossman (2000) is about 2×10^{-5} bars. The choice fO_2 ~ IW-1.5 is required by the FeO/(FeO+MgO) of olivine in ordinary chondrites Grossman (2010). The ideal gas law can be used to convert a partial pressure of potassium of 2×10^{-5} bars to a concentration of 1.2×10^{-4} moles/m^3. We will assume that a typical Type IA chondrule had a solar proportion of K_2O to Al_2O_3 to begin with (~0.13 wt% K_2O) and that it then lost 0.1 wt% K_2O by evaporation. This would have transferred about 2×10^{-5} moles of potassium to the gas for each gram of chondrule. This results in an estimate that about ten grams of chondrule per meter cubed would have been required to achieve saturation, which is comparable to the lower end of the range of chondrule densities estimated by Alexander et al. (2008) based on a similar argument for sodium saturation. Our estimate is, on the other hand, orders of magnitude larger than the chondrule densities estimated by Ciesla et al. (2004) based on a calculation of the number density of chondrules required to account for the observed proportion (~5%) of compound chondrules. There are admittedly very large uncertainties involved in any such an estimate (see discussion in Ciesla et al. 2004 and 2006), so we are not yet ready to conclude that our estimate of ten grams of Type IA chondrule precursor per m^3 should be ruled out based on the observed proportion of compound chondrules. The larger point is that the compound chondrules provide an independent argument for chondrules having been partially molten in regions of high chondrule volume density.

A relevant question is whether partial evaporation of Na_2O and K_2O from chondrules to the point where the surrounding gas becomes saturated in sodium and potassium is consistent with the requirement of fO_2~IW-1.5 (Grossman, 2010). For the present argument, we assume this value for the fO_2 of the gas in equilibrium with partially molten Type IA chondrules and temperatures in the range 1743K-2043K. Using a thermodynamic model for the equilibrium between a Type IA-like liquid and surrounding gas we find that if chondrules had partially evaporated into an initially very low pressure surrounding gas ($P<10^{-7}$ bars), the conditions would have become unacceptably oxidizing (~ IW+4). If, however, the Type IA chondrules had been surrounded by an equilibrium speciated hydrogen-dominated gas at $P\sim10^{-2}$ bars and

T=2043 K (or P~4×10^{-4} bars at T=1743 K) the equilibrium fO_2 would have been very close to IW-1.5. This range of gas pressures is not inconsistent with the pressure associated with the passage of a shock wave as calculated by Desch and Connelly (2002). However we have not taken into account that during the passage of a shock the hydrogen would have become somewhat more dissociated than at equilibrium making it more effectively reducing. Thus hydrogen pressures somewhat higher than those calculated above assuming equilibrium speciation would have been sufficient to meet the requirement of log fO_2~IW-1.5.

In order for a chondrule that maintains equilibrium with its surrounding gas to also loose some fraction of its volatile components, the gas must be removed from the vicinity of the chondrule or else the evaporated sodium and potassium would simply recondense as the system cools. Richter (2004) showed that a key parameter that determines the effect of gas removal on the elemental and isotopic fractionation of the residue is the ratio of the evaporation time scale τ_{evap} (moles K per chondrule/evaporation rate times surface area) to the residence time (τ_{res}) of the gas in the vicinity of the evaporating source. When the ratio τ_{evap}/τ_{res} is ten or greater (i.e., slow evaporation relative to gas removal), the elemental and isotopic fractionations become much the same as for free evaporation into vacuum. When the ratio of these timescales is small (< 0.1) the system looses volatile components as the surrounding gas is slowly removed but remains sufficiently close to equilibrium at all times so that there is little isotopic fractionation of the eventual residue (see Fig. 16 in Richter 2004). At T=1943 K and fO_2=IW, the potassium evaporation time τ_{evap} for a 1 mm chondrule with 0.2 wt % potassium is about 0.2 seconds. The residence time of gas in the vicinity of a chondrule will be of order $V^{1/3}/u$ where V is the volume saturated by one mm-size chondrule (~50 cm^3) and u is the velocity of the gas relative to the chondrule. The condition $\lambda=\tau_{evap}/\tau_{res} < 0.1$ would require velocities of a cm per second or less. The smallness of the calculated velocity required for equilibrium is a consequence of an unrealistic assumption that the gas leaving the vicinity of the chondrule is continuously replaced by gas effectively devoid of volatiles. Had we considered the case where the gas surrounding nearby chondrules is also saturated in volatiles, then there might be no difference between the gas replacing the gas being removed from a given chondrule and thus the system would appear to be effectively closed regardless of the gas flow velocity. This line of reasoning leads to the conclusion that in order for chondrules to loose some fraction of their volatile components without associated isotopic fractionation requires spatial gradients in saturation vapor pressures. This was the case in our experiments where we evaporated a chondrule-like liquid in a flowing gas stream and it could also be true of how chondrules might have lost a fraction of their more volatile components. The mass conservation equations for a chondrule-like liquid evolving in a thermodynamic gradient given in the Appendix provide a formalism for establishing what aspects of the results of the laboratory experiments are relevant for understanding processes that might have affected the elemental and isotopic compositions of actual chondrules.

Estimating the various time scales that determine how chondrules would have evolved requires specifying parameters that are not well known and thus a broad range for these will be considered to reflect the uncertainty of their actual values in the

chondrule-forming region. For the environmental conditions we will consider T=1943 K and a total gas pressure of 10^{-3} bars. For the gas volume per chondrule, V_c, we will use both 10^3 cm^3 (similar to our estimate) and a much larger value of 10^6 cm^3. A chondrule radius a = 0.05 cm is assumed. The saturation vapor pressure of potassium at T=1943 K over a chondrule-like liquid with 0.23wt% K_2O and log$f$O$_2$=-8.83 (IW-1.5) was calculated using the thermodynamic model of Ebel and Grossman (2000) to be $P_{i,o}^{sat} = 2.5\times10^{-5}$ bars ($\rho_{i,0}^{sat} = 1.6\times10^{-9}$ moles/cm^3). The evaporation rate of potassium for these conditions is $J_{i,o}$=5.8×10^{-6} moles per cm^2 per second. The saturation times ($\tau_{sat} = \frac{V\rho_{i,o}^{sat}}{J_{i,o}4\pi a^2}$, see Appendix) are 8 seconds and 8000 seconds for V=V_c=10^3 cm^3 and 10^6 cm^3 respectively. The saturation time scale does not depend on the fO$_2$ or the amount of potassium in the melt because both the molar density of potassium and the evaporation rate have similar dependence on these two quantities. In order to compare the saturation time scale to the other time scales over which the melt would evolve requires specifying a length scale in the chondrule-forming region over which the saturation vapor pressure varies. The most likely cause of changes in saturation is large-scale temperature gradients, with about an order of magnitude change in saturation vapor pressure for a 200K change in temperature. The relevant length scale might be that of the region of high chondrule density, which Cuzzi and Alexander (2006) have argued is of the order of 150 km to 6000 km. Another possible measure might be the length scale over which the high temperatures associated with a shock vary by 200K, which is of the order of several 1000 km in the shock-heating calculations for high chondrule density by Desch and Connelly (2002). The diffusion of potassium in a gas at T=1943 K and P=10^{-3} bars is of the order of D=10^4 cm^2/s (see parameterization for D given earlier). This results in the diffusive time scale ($\tau_{diff} = \frac{L^2\rho_o}{D\rho_{i,o}^{sat}V_r} \approx \frac{L^2}{D}$, see Appendix) being of the order of 10^{10} seconds and 10^{13} seconds for choices of the length scale of 100 km and 5000 km. Estimating the advection time τ_{adv} requires specifying a gas flow relative to the chondrule for which we will use U=1 cm/sec which is likely a lower bound for the outward velocity of chondrules relative to the gas. Even ignoring turbulence and transport by eddy diffusion away from regions of high chondrule density, an outward velocity of at least a cm/sec would have been required for any chondrules to survive the tendency of small particles to drift towards the sun on a timescale of the order of only a few tens of thousands of years (Weidenschilling, 1977; see also Cuzzie et al., 2005)). This results in $\tau_{adv} = \frac{L}{U} \approx 1\times10^7$ seconds and 5×10^8 seconds for the length scales of 100 km and 5000 km respectively. Thus for a system with large chondrule densities, the saturation time scale is by far the shortest and thus the system would be close to equilibrium at all times. The Peclet number Pe=UL/D will be of order 10^3 or 5×10^4 when the saturation vapor pressure varies over a length scale of either 100 km or 5000 km. The key point is that regardless of a very large range in velocities and length scales assumed, the transport of volatile species in the regions of enhanced chondrule volume density will be overwhelmingly by advection, and thus isotopic fractionation by diffusion in the gas will be insignificant.

We think the most likely explanation of the fact that the Type IIA and Type IA chondrules from Semarkona retain some measurable sodium and potassium with no systematic isotopic fractionation of the potassium is that while molten these chondrules were in a region of sufficiently high chondrule volume density that partial evaporation or condensation of the volatile components was sufficient to maintain a saturated surrounding gas. This is an idea that was used by Alexander et al. (2000) to explain the lack of potassium isotopic fractionation of Bishampur chondrules, by Alexander and Grossman (2005) in their discussion of the potassium isotopic composition of Semarkona chondrules, and most recently by Alexander et al. (2008) to explain the apparent lack of sodium loss by evaporation while olivine was crystallizing in molten chondrules. What has not been adequately addresses is the need for transport of the equilibrated gas relative to the molten chondrules The observation that the Type IIA chondrules are somewhat enriched in sodium and potassium relative to the more refractory elements when compared to the solar composition could be explained by condensation of the volatile components transported from a region of higher temperature and thus higher vapor pressure than the local saturation pressure (see Georges et al., 2000 for a laboratory example of this process). If this transport were dominantly by a sufficiently slow advection of the saturated gas, the isotopic fractionation of the recondensed volatiles would be negligible. The Type IA chondrules on the other hand are in most cases significantly depleted in sodium and potassium, which could have been accomplished by the saturated gas interacting with these chondrules having come from cooler regions and thus would have lower partial pressure of sodium and potassium than the saturation vapor pressure at the temperature of the chondrule. Again, if the transport of volatiles is by sufficiently slow advection, there would be no isotopic fractionation associated with the loss of volatiles from the chondrule precursor. These processes could explain the abundances of sodium and potassium in the Type IIA and Type IA chondrules from Semarkona.

ACKNOWLEDGMENTS

This work was supported by the NASA Cosmochemistry Program through grant NNG06GE85G (RAM, FMR). The ongoing collaboration between Frank Richter, John Christensen, and Amy Gaffney is supported by the Director, Office of Science, Office of Basic Energy Sciences, of the U.S. Department of Energy through grants (under contracts DE-FG02-01ER15254,A005 and DE-AC02-05CH11231). We thank Bruce Watson of the Rensselaer Polytechnic Institute for the diffusion experiment used in this study to determine the diffusivity of potassium in a chondrule-like melt. We also thank Rachel Lindvall of the Lawrence Livermore National Laboratory for her help with the ICP-MS measurements. We thank Conel Alexander and Herbert Palme for their detailed reviews of the original manuscript, which resulted in a much improved final version of the paper.

Table 1. Properties of evaporation residues

Sample	T °C	Gas, fO_2	Minutes	surface mm^2 (initial/final)	SiO2, wt%	MgO, wt%	Al_2O_3, wt%	CaO, wt%	Na_2O, wt%	K_2O, wt%	FeO, wt%	$\delta^{41}K$(‰)	2σ
IIAB1 start					60	22	4.0	2.2	3.5	3.5	5		
IIAB1-1	1470	Vacuum	30	39.7 / 30.0	62.21	23.68	5.01	2.68	0.16	1.15	5.49	28.47	0.48
IIAB1-2	1470	Vacuum	30	30.3 / 26.6	62.48	23.02	4.79	2.57	0.05	0.68	5.75	37.1	0.5
IIAB1- 3	1470	Vacuum	60	32.5 / 27.4	62.94	23.78	4.79	2.55	<0.01	0.21	5.44	62.75	0.81
IIAB1-4	1470	Vacuum	45	32.8 / 27.5	62.68	23.20	4.83	2.60	0.01	0.40	5.67	48.24	0.53
IIAB1-5	1470	Vacuum	15	27.1 / 25.5	61.90	22.97	4.67	2.49	0.33	1.37	5.52	19.82	0.68
IIAB1-6	1470	Vacuum	0	25.7 / 25.2	60.24	21.67	4.36	2.33	2.42	3.03	4.95	2.06	0.53
IIAB1-7	1470	Vacuum	45	39.3 / 29.9	62.76	22.91	4.64	2.46	0.03	0.57	5.66	38.63	1.05
IIAB1-8	1470	Vacuum	20	27.9 / 25.6	61.92	23.38	4.85	2.57	0.16	1.09	5.57	26.42	0.78
IIAB1-9	1470	Vacuum	0	29.0 / 26.6	60.48	21.49	4.54	2.50	2.75	3.33	5.03	1.25	0.33
IIAB2-1	1470	Vacuum	10	21.8 / 21.5	52.32	27.42	4.92	3.57	0.06	0.08	11.75		
IIAB2-2	1470	Vacuum	20	24.6 / 24.3	52.61	27.15	4.96	3.60	0.02	0.04	11.73		
IIAB2-3	1470	Vacuum	30	26.2 / 25.3	52.38	27.78	4.88	3.54	0.03	0.00	11.49		
IIAB2-4	1470	Vacuum	0	20.2 / 20.2	51.64	27.79	4.66	3.41	0.88	0.34	11.55		
IIAB2-5	1470	Vacuum	5	21.1 / 20.9	51.75	28.47	4.61	3.42	0.30	0.18	11.48		
IIAB2-6	1470	Vacuum	15	23.3 / 23.0	52.84	26.40	5.11	3.73	0.02	0.06	11.99		
IIAB2-7	1470	Vacuum	25	25.2 / 24.8	53.07	26.34	5.18	3.75	0.00	0.02	11.77		
IIAB2-11	1470	Vacuum	15	24.3 / 23.9	51.81	27.94	4.64	3.44	0.02	0.04	11.79		
IIAB2-12	1470	Vacuum	5	21.9 / 21.6	51.68	27.63	4.73	3.55	0.29	0.16	11.78		
IIAB2-13	1470	Vacuum	0	22.3 / 22.1	49.94	27.85	4.41	3.45	1.78	0.51	12.46		
IIAB2-15	1470	Vacuum	0	19.9 / 19.7	49.49	28.11	4.43	3.45	1.78	0.45	12.62		
IIAB2-17	1470	Vacuum	10	22.5 / 22.2	52.47	26.31	4.93	3.74	0.23	0.13	12.14		
IIAB2-23	1470	Vacuum	5	21.5 / 21.2	53.17	23.57	5.15	4.32	0.24	0.16	13.29		
IIAB2-28	1470	Vacuum	5	26.3 / 26.1	52.16	24.93	5.03	4.09	0.80	0.28	12.86		
IIAB2-29	1470	Vacuum	10	24.4 / 24.0	52.10	26.05	4.94	3.90	0.06	0.06	12.68		
				gas flow rate									
IIAB2-14	1470	H_2-CO_2, IW+2.5	720	24 cm/min	51.89	30.27	4.10	3.28	0.16	0.04	10.05		
IIAB2-16	1470	H_2-CO_2, IW+2.5	5	24 cm/min	49.67	27.68	4.33	3.47	2.37	0.41	12.36		
IIAB2-18	1470	H_2-CO_2, IW+2.5	388	24 cm/min	51.27	30.33	4.06	3.17	0.52	0.11	10.42		
IIAB2-19	1470	H_2-CO_2, IW+2.5	7	24 cm/min	49.66	27.62	4.33	3.34	2.10	0.34	12.47		
IIAB2-20	1470	H_2-CO_2, IW+2.5	118	24 cm/min	50.88	29.13	4.12	3.37	1.18	0.24	11.11		
IIAB2-27	1470	H_2-CO_2, IW+2.5	87	24 cm/min	51.73	25.97	4.47	3.88	1.13	0.20	12.36		
IIAB5-start					55	15	3	2	5	5	15	0.00	
IIAB5-1	1432	H_2-CO_2, IW+2.5	30	24 cm/min	57.14	14.51	2.99	1.97	4.25	3.91	14.25		
IIAB5-2	1432	H_2-CO_2, IW+2.5	60	24 cm/min	57.24	14.85	2.97	2.04	3.94	3.52	14.71		
IIAB5-3	1432	H_2-CO_2, IW+2.5	45	24 cm/min	57.65	14.88	2.96	2.01	4.07	3.77	14.51		
IIAB5-4	1432	H_2-CO_2, IW+2.5	15	24 cm/min	56.01	14.7	2.97	1.97	4.33	3.91	14.81		
IIAB5-18	1426	H_2-CO_2, IW+2.5	2155	24 cm/min	63.69	16.72	3.45	2.28	0.56	0.81	12.53	10.6	0.53
IIAB5-20	1426	H_2-CO_2, IW+2.5	1442	24 cm/min	62.36	16.62	3.38	2.27	0.65	1.04	13.12	8.92	0.38
IIAB5-15	1426	H_2-CO_2, IW+2.5	731	24 cm/min	62.58	16.35	3.32	2.22	0.83	1.37	13.35	8.15	0.44
IIAB5-19	1427	H_2-CO_2, IW+2.5	2	24 cm/min	56.44	14.96	3.16	2.06	4.56	4.03	14.12	0.07	0.35
IIAB5-21	1427	H_2-CO_2, IW+2.5	360	24 cm/min	59.44	16.32	3.18	2.19	1.33	1.85	15.06	6.36	0.35
IIAB5-22	1427	H_2-CO_2, IW+2.5	180	24 cm/min	57.87	15.61	3.12	2.08	2.17	2.49	15.42		
50Di50Le-0		air	0	0	55.21	6.17	15.61	8.59		14.42		0.00	
50Di50Le-5	1400	H_2	<105*	70 cm/min	55.16	7.98	22.12	13.16		1.59			
50Di50Le-1	1412	H_2	<180*	70 cm/min	58.03	7.74	20.32	12.38		1.52			
50Di50Le-2	1400	H_2	<210*	70 cm/min	58.15	7.83	20.05	12.35		1.62		2.91	0.24
50Di50Le-9	1450	H_2	<170*	70 cm/min	58.58	7.40	18.84	11.66		3.53		3.64	0.49
50Di50Le-10	1450	H_2	60	70 cm/min	51.64	8.79	24.57	14.78		0.23		5.09	0.40
50Di50Le-12	1450	H_2	31	70 cm/min	56.26	7.69	21.85	12.53		1.68		4.03	0.35
50Di50Le-3	1450	He	780	70 cm/min	58.20	6.10	16.20	9.40		10.17		0.65	0.47
50Di50Le-7	1450	He	2520	70 cm/min	59.70	6.50	16.70	9.98		7.13		1.32	0.53
50Di50Le-6	1450	He	295	70 cm/min	57.15	6.12	15.72	9.51		11.51		0.59	0.30

* - Sample self-quenched at some time before end of run

Table 2. Estimates of the evaporation coefficients of sodium and potassium for vacuum experiments starting from the ABII1 composition and eight starting from the lower potassium ABII2 composition. Also shown for comparison are estimates made by Fedkin et al (2006) and by Alexander (2002).

Sample	T(˚C)	Pressure	γ_K	γ_{Na}	source*
IIAB-1	1470	$<10^{-6}$ Torr	0.051	0.065	1
IIAB-2	1470	$<10^{-6}$ Torr	0.081	0.067	1
IIAB-5	1470	$<10^{-6}$ Torr	0.062	0.091	1
IIAB-8	1470	$<10^{-6}$ Torr	0.050	0.062	1
Ave ± Std dev			0.061±.014	0.071±.013	1
IIAB2-1	1470	$<10^{-6}$ Torr	0.22	0.09	1
IIAB2-5	1470	$<10^{-6}$ Torr	0.18	0.10	1
IIAB2-6	1470	$<10^{-6}$ Torr	0.17	0.07	1
IIAB2-12	1470	$<10^{-6}$ Torr	0.29	0.21	1
IIAB2-17	1470	$<10^{-6}$ Torr	0.18	0.12	1
IIAB2-23	1470	$<10^{-6}$ Torr	0.28	0.22	1
IIAB2-28	1470	$<10^{-6}$ Torr	0.14	0.15	1
IIAB2-29	1470	$<10^{-6}$ Torr	0.30	0.15	1
Ave ± Std dev			0.22±.06	0.14±.05	1
C1	1450	$1x10^{-5}$ bar air	0.13±.02	0.26±.05	2
C1	1450	$9x10^{-5}$ bar H_2	0.017±.002	0.042±.020	2
Not reported	1450	$\sim10^{-5}$ bar air	0.12	0.12	3

C1: Composition 1 of Yu et al. (2003).
*(1) This work (2) Fedkin et al., 2006 (3) Alexander, 2002 using his equilibrium reference model (EQR) to fit data from Yu and Hewins (1997)

APPENDIX

A mathematical model for the evolution of a chondrule in a large-scale thermodynamic gradient will involve a conservation equation for the abundance of that species in the chondrule and in a volume V of surrounding gas. The conservation equation for the volatile species i in a chondrule of radius a is

$$\frac{4\pi a^3}{3}\frac{\partial}{\partial t}\rho_{i,chond} = -J_{i,o}4\pi a^2(1-\frac{\rho_{i,gas}}{\rho_i^{sat}}) \qquad \text{(A1)}$$

where $\rho_{i,chond}$ is the molar density of i in the chondrule, $\rho_{i,gas}$ is the molar density of i at the surface of the chondrule and ρ_i^{sat} is the saturation vapor pressure of i over the chondrule. $J_{i,o}$ is the free evaporation rate (i.e., in the limit $\rho_{i,gas} << \rho_i^{sat}$). Because the evaporation only involves minor components, the radius is assumed to be unchanging for the purpose of Eqn. A1. The conservation equation for i in a gas volume V is

$$\frac{d}{dt}\int_V \rho_{i,gas}dv = -\int_\Sigma \rho_{i,gas}\hat{u}\bullet\hat{n}ds + \int_\Sigma D\nabla\rho_{i,gas}\bullet\hat{n}ds + J_{i,o}4\pi a^2(1-\frac{\rho_{i,gas}}{\rho_i^{sat}}) \qquad \text{(A2)}$$

where Σ is the surface enclosing V, $\hat{n}$ is the outward normal to Σ, $\hat{u}$ is the velocity of gas relative to the fixed volume V, and D is the diffusion coefficient of i in the gas. The surface integrals can be converted into volume integrals using the divergence theorem, thus Eqn. A2 becomes

$$\frac{d}{dt}\int_V \rho_{i,gas}dv = -\int_V \nabla\bullet(\rho_{i,gas}\hat{u})dv + \int_\Sigma D\nabla^2\rho_{i,gas}dv + J_{i,o}4\pi a^2(1-\frac{\rho_{i,gas}}{\rho_i^{sat}}) \qquad \text{(A3)}$$

For simplicity, we will consider the volume per chondrule to be a cube of dimension L, that $\hat{u} = U$ in the x direction and that $\nabla\rho_{i,gas} = \frac{\partial}{\partial x}\rho_{i,gas}$. Equation A3 becomes

$$L^3\frac{\partial}{\partial t}\rho_{i,gas} = -L^3U\frac{\partial}{\partial x}\rho_{i,gas} + L^3D\frac{\partial^2}{\partial x^2}\rho_{i,gas} + J_{i,o}4\pi a^2(1-\frac{\rho_{i,gas}}{\rho_i^{sat}}) \qquad \text{(A4)}$$

(A1) and (A4) can be combined to give an equation for the total amount of i in V.

$$\frac{4\pi a^3}{3}\frac{\partial}{\partial t}\rho_{i,chond} + L^3\frac{\partial}{\partial t}\rho_{i,gas} = -L^3U\frac{\partial}{\partial x}\rho_{i,gas} + L^3D\frac{\partial^2}{\partial x^2}\rho_{i,gas} \qquad \text{(A5)}$$

The relative importance of the various terms is best judged when (A5) is nondimensionalized using $t = \tau t' \ni \frac{\partial}{\partial t} \to \frac{1}{\tau}\frac{\partial}{\partial t'}$, $x = L x' \ni \frac{\partial}{\partial x} \to \frac{1}{L}\frac{\partial}{\partial x'}$, $\rho_{i,chond} = \rho_o\rho'_{i,chond}$, $\rho_{i,gas} = \rho_{i,o}^{sat}\rho'_{i,gas}$, where ρ_o is the initial molar density of i in the chondrule and $\rho_{i,o}^{sat}$ is the corresponding saturation vapor pressure of i. The primed variables are nondimensional and if the scaling has been chosen appropriately, the primed

variables will be order one and the relative magnitude of the various terms can be judged by the quantities multiplying the primed variables. We also define a nondimensional quantity $V_r = 3L^3/4\pi a^3$, which is the volume ratio of the gas to that of the chondrule. Substitution these relationships into (A5) gives

$$\frac{\partial}{\partial t'}\rho'_{i,chond} + \frac{V_r\rho^{sat}_{i,o}}{\rho_o}\frac{\partial}{\partial t'}\rho'_{i,gas} = -\frac{L^2U\tau\rho^{sat}_{i,o}}{(4\pi a^3/3)\rho_o}\frac{\partial}{\partial x'}\rho'_{i,gas} + \frac{LD\tau\rho^{sat}_{i,o}}{(4\pi a^3/3)\rho_o}\frac{\partial^2}{\partial x'^2}\rho'_{i,gas} \qquad \text{(A6)}$$

choosing the time scale $\tau = \frac{L^2\rho_o}{D\rho^{sat}_{i,o}V_r}$, (A6) becomes

$$\frac{\partial}{\partial t'}\rho'_{i,chond} + \frac{V_r\rho^{sat}_{i,o}}{\rho_o}\frac{\partial}{\partial t'}\rho'_{i,gas} = -P_e\frac{\partial}{\partial x'}\rho'_{i,gas} + \frac{\partial^2}{\partial x'^2}\rho'_{i,gas} \qquad \text{(A7)}$$

This choice of τ is effectively the diffusive time scale L^2/D because the quantity $\frac{\rho_o}{\rho^{sat}_{i,o}V_r}$ is order one when partial evaporation saturates the environment. $P_e = UL/D$ is a Peclet number corresponding to the ratio of the diffusion time scale to the advection time scale L/U. A large Peclet number indicates that advection is the dominant process removing the volatile species from the vicinity of the molten sample. Assuming that the activity of i in the condensed phase is for practical purposes Henrian at low concentrations, as is the case of potassium in a chondrule-like melt, the ratio $\rho_{i,chond}/\rho_{i,gas} \approx \rho_o/\rho^{sat}_{i,o}$, and thus $\rho'_{i,gas} \approx \rho'_{i,chond}$. A(7) can then be further simplified to give the following equation for the evolution of the chondrule molar density.

$$(1 + \frac{V_r\rho^{sat}_{i,o}}{\rho_o})\frac{\partial}{\partial t'}\rho'_{i,chond} = -P_e\frac{\partial}{\partial x'}\rho'_{i,gas} + \frac{\partial^2}{\partial x'^2}\rho'_{i,gas} \qquad \text{(A8)}$$

The development leading to Eqn. A8 is based on a nondimensionalization of the molar density in the gas that requires that it be close to saturation. This in turn requires that the time it takes to saturate the volume V be short compared to the time scale used to nondimensionalize time. The saturation time scale can be estimated by balancing the term on the left hand side by the evaporation term on the right hand side of Eqn. (A3). This results in the following balance

$$\frac{d}{dt}\int_V \rho_{i,gas}dv = J_{i,o}4\pi a^2(1 - \frac{\rho_{i,gas}}{\rho^{sat}_i}) \qquad \text{(A9)}$$

which can be approximated as

$$V\frac{d}{dt}(1 - \frac{\rho_{i,gas}}{\rho^{sat}_{i,o}}) = -\frac{J_{i,o}4\pi a^3}{\rho^{sat}_{i,o}}(1 - \frac{\rho_{i,gas}}{\rho^{sat}_{i,o}}) \qquad \text{(A10)}$$

which for an initial condition $\rho_{i,gas} = 0$ has solution $\rho_{i,gas} = \rho_{i,o}^{sat}(1 - e^{-\lambda t})$ with $\lambda = \frac{J_{i,o} 4\pi a^2}{V \rho_{i,o}^{sat}}$ giving an estimate of the saturation time $\tau_{sat} = \lambda^{-1} = \frac{V \rho_{i,o}^{sat}}{J_{i,o} 4\pi a^2}$.

The potassium saturation time in the one-bar tube furnace evaporation experiments is about 1 second at T=1743 K calculated using a furnace volume V=500cm^3, a=0.125cm, $\rho_{i,0}^{sat} = P_{i,o}^{sat}/(RT) = 4.7\times10^{-12}$ moles/cm^3 taken from a thermodynamic calculation with 0.31 wt% K_2O, and $J_{i,o}$=1.9×10^{-8} mole/cm^{2}s for log fO_2=-5.75 using the parameterization given in the text. The estimate of the evaporation time does not depend on the actual value of fO_2 because $J_{i,o}$ and $\rho_{i,0}^{sat}$ have the same dependence on the oxygen fugacity. The diffusive equilibration time τ_{diff} for the one-bar H_2+CO_2 experiments is about 40 seconds ($\tau_{diff} = L^2/D$) for L=20 cm and D ~10 cm^2/s calculated using the parameterization $D \approx 1.4 \times 10^{-4}\ T^{3/2}/P$ (Richter et al., 2002) where T is temperature in Kelvin and P is the total gas pressure in bars. The advection time scale τ_{adv} (=L/U) is about 20 seconds for L=20 cm and a gas flow velocity U~1cm/s. For these conditions the saturation time is much shorter than either the advection or diffusion time scales, thus the one bar evaporation experiments are in the limit of transport of a saturated gas away from a molten sample. The Peclet number $Pe=UL/D$ for the one-bar experiments is about two, signifying that both advection and diffusion are important in transporting potassium away from the evaporating chondrule-like liquid.

Using the equations and definitions given above to estimate the various time scales that might apply to actual chondrules is more problematic than in the case of a laboratory experiment because many of the quantities that have to be specified are not well known even as to their order of magnitude. A discussion of possible values for these parameters and the implications for how olivine-rich chondrules would have evolved is given in the main text.

References.

Alexander C.M.O'D. 2002. Application of MELTS to kinetic evaporation models of FeO-bearing silicate melts. *Meteoritics & Planetary Science* 37:245-256.

Alexander C.M.O'D., Grossman J.N., Wang J., Zanda B., Bourot-Denise M., and Hewins R.H. 2000. The lack of potassium-isotopic fractionation in Bishunpur chondrules. *Meteoritics & Planetary Science* 35:859-868.

Alexander C.M.O'D. and Wang J. 2001. Iron isotopes in chondrules: Implications for the role of evaporation during chondrule formation. *Meteoritics & Planetary Science* 36:419-428.

Alexander C. M. O'D. and Grossman J. N. (2005) Alkali elemental and potassium isotopic compositions of Semarkona chondrules. *Meteoritics & Planetary Science* 40:541–556.

Alexander C. M. O'D., Grossman J. N., Ebel D. S. and Ciesla F. J. 2008. The formation conditions of chondrules and chondrites. *Science* 320:1617–1619.

Beckett J. R. 1986. The origin of calcium-, aluminum-rich inclusions from carbonaceous

chondrites: An experimental study. Ph.D. thesis, University of Chicago, Chicago.
Beckett J.R., Live D., Tsay F-D., Grossman L., and Stolper E. 1988. Ti^{3+} in meteoritic and synthetic hibonite. *Geochimica et Cosmochimica Acta* 52:1479-1495.
Borisov A., Pack A., Kropf A., and Palme H. 2008. Partitioning of Na between olivine and melt: An experimental study with application to the formation of meteoritic Na2O-rich chondrule glass and refractory forsterite grains. *Geochimica et Cosmochimica Acta* 72:5558-5573.
Ciesla F.J., Lauretta D.S., and Hood L.L. 2004. The frequency of compound chondrules and implications for chondrule formation. *Meteorit. Planet. Sci.* 39:531-544.
Clayton R. N., Hinton R. W., and Davis A. M. 1988. Isotopic variations in the rock-forming elements in meteorites. *Philosophical Transactions Royal Society of London* A325:483–501.
.Cohen B.A., Hewins R.H., Alexander C.M.O'D. 2004. The formation of chondrules by open-system melting of nebular condensates. *Geochimica et Cosmochimica Acta* 68:1661-1675.
Cuzzi J.N. and Alexander C.M .O. 2006. Chondrule formation in particle-rich nebular regions at least hundreds of kilometers across. *Nature* 441:483-485.
Cuzzi, J. N., Ciesla F.J., Petaev, M.I., Krot A.N., Scott E.R.D., and Weidenschilling, S.J. 2005. Nebular evolution of thermally processed solids: Reconsiling models and meteorites. In *Chondrites and the Protoplanetary Disk*, edited by Krot A.N., Scott E. R. D., and Reipurth B. *ASP Conference Series,* 341:732-773.
Dauphas N., Janney P. E., Mendybaev R. A., Wadhwa M., Richter F. M., Davis A. M., van Zuilen A., Hines R., and Foley C. N. 2004. Chromatographic separation and multicollection-ICPMS analysis of iron. Investigating mass-dependent and –independent isotope effects. *Analitical Chemistry* 76:5855–5863.
Davis A. M., Hashimoto A., Clayton R. N., and Mayeda T. K. 1990. Isotope mass fractionation during evaporation of forsterite (Mg_2SiO_4). *Nature* 347:655–658.
Desch S. J. and Connolly H. C., Jr. 2002. A model of the thermal processing of particles in solar nebula shocks: Applications to the cooling rate of chondrules. *Meteoritics & Planetary Science* 37:183–202.
Ebel D.S. and Grossman L. 2000. Condensation in dust-enriched systems. *Geochimica et Cosmochimica Acta* 64:339-366.
Fedkin A. V., Grossman L., and Ghiorso M. S. 2006. Vapor pressures and evaporation coefficients for melts of ferromagnesian chondrule-like compositions. *Geochimica et Cosmochimica Acta* 70:206–223.
Galy A., Young E.D., Ash A.D., and O'Nions K.R. 2000. The formation of chondrules at high gas pressures in the solar nebula. *Science* 290:1751-1753.
Galy A., Belshaw N. S., Halicz L., and O'Nions R. K. 2001. High-precision measurement of magnesium isotopes by multiple-collector inductively coupled plasma mass spectrometry. *International Journal of Mass Spectrometry* 208:89–98.
Georges P., Libourel G., and Deloule E. 2000. Experimental constraints on alkali condensation in chondrule formation. *Meteoritics & Planetary Science* 35:1183-1188.
Grossman L. 1972. Condensation in the primitive solar nebula. *Geochimica et Cosmochimica Acta* 36:597–619.
Grossman L. 2010. Vapor-condensed phase processes in the early solar system.

Meteoritics & Planetary Science 45:7-20.
Grossman J. N. and Wasson J. T. 1983. The compositions of chondrules in unequilibrated chondrules: An evaluation of theories for the formation of chondrules and their precursor materials. In *Chondrules and their Origins*, edited by King E. A., Houston, Lunar and Planetary Institute. pp. 88-121.
Hashimoto A. 1990. Evaporation kinetics of forsterite and implications for the early solar nebula. *Nature* 347:53–55.
Hirth J. P. and Pound G. M. 1963. *Condensation and Evaporation Nucleation and Growth Kinetics*. Macmillan, New York, 191 p.
HewinsR.H. and Radomsky P.M. (1990) Temperature conditions for chondrule formation. *Meteoritics* 25:309-318.
Jones R. H. 1990. Petrology and mineralogy of Type II, FeO-rich chondrules in Semarkona (LL3.0): Origin by closed-system fractional crystallization, with evidence for supercooling. *Geochimica et Cosmochimica Acta* 54:1785–1802.
Jones R.H. and Lofgren G.E. 1993. A comparison of FeO-rich porphyritic olivine chondrules in unequilibrated chondrites and experimental analogues. *Meteoritics & Planetary Science* 38:213-221.
Jones R.H. and Scott E.R.D. 1989. Petrology and thermal history of Type IA chondrules from Semarkona (LL3.)) chondrite. *Procedings of the Lunar and Planetary Science Conference* 19:523-536.
Knight K.B.**,** Kita N., Mendybaev R.A., Richter F., Davis A.M., and Valley J.W. 2009. Silicon isotopic fractionation of CAI-like vacuum evaporation residues. *Geochimica et Cosmochimica Acta* 73:6390-6401.
Kuroda D. and Hashimoto A. 2002. The reaction of forsterite with hydrogen—its apparent and real temperature dependences. *Antarctic Meteorites XXV*: 64–66.
Mendybaev R. A., Beckett J. R., Stolper E., and Grossman L. 1998. Measurement of oxygen fugacities under reducing conditions: non-Nernstian behavior of Y_2O_3-doped zirconia oxygen sensors. *Geochimica et Cosmochimica Acta* 62:3131–3139.
Mendybaev R.A., Richter F.M., and Davis A.M. 2006. Crystallization of melilite from CMAS-liquids and the formation of melilite mantle of Type B1 CAIs: Experimental simulations. *Geochimica et Cosmochimica Acta* 70:2622-2642.
Nagahara H. and Ozawa K. 1996. Evaporation of forsterite in H-2 gas. *Geochimica et Cosmochimica Acta* 60:1445-1459.
Nuth J.A., Furguson F.T., Johnson N., and Martinez D. 2003. Initial measurements of the vapor pressure of simple refractory materials: Cu and Fe (abstract #1598). 34th Lunar and Planetary Science Conference.
Palme H. and Jones A. 2004. Solar system abundances of the elements. In *Meteorites, Planets, and Comets*, edited by Davis A. M., Vol. 1 *Treatise on Geochemistry,* edited by Holland H. D. and Turekian K. K. Oxford: Elsevier-Pergamon. pp. 41–61.
Radomsky P.M. and Hewins R.H. 1990. Formation conditions of pyroxene-olivine and magnesian-olivine chondrules. *Geochimica et Cosmochimica Acta* 54:3475-3490.
Richter F.M. 2004. Timescales determining the degree of kinetic isotope fractionation by evaporation and condensation. *Geochimica et Cosmochimica Acta* 68:4971-4992.
Richter F. M., Davis A. M., Ebel D. S., and Hashimoto A. 2002. Elemental and isotopic fractionation of Type B calcium-, aluminum-rich inclusions: experiments,

theoretical considerations, and constraints on their thermal evolution. *Geochimica et Cosmochimica Acta* 66:521–540.

Richter F.M., Davis A.M., DePaolo D.J. and Watson E.B. 2003. Isotope fractionation by chemical diffusion between molten basalt and rhyolite. *Geochimica et Cosmochimica Acta* 67:3905-3923.

Richter F.M., Mendybaev R.A., and Davis A.M. 2006. Conditions in the protoplanetary disk as seen by the type B CAIs. *Meteoritics & Planetary Sci*ence 41:83-93.

Richter F.M., Mendybaev R.A., Christensen J., Gaffney A., and Ebel D. 2009a. Elemental and isotopic fractionation of chondrule-like liquids by evaporation into vacuum (abstract #2321). 40th Lunar and Planetary Science Conference.

Richter F.M., Watson E.B., Mendybaev R., Dauphas N., Georg B., Watkins J., and Valley J. 2009b. Isotopic fractionation of the major elements of molten basalt by chemical and thermal diffusion. *Geochimica et Cosmochimica Acta* 73:4250-4263.

Rubin A. E. 2000. Petrologic, geochemical and experimental constraints on models of chondrule formation. *Earth-Science Reviews* 50:3-27.

Scott E. R. D. and Krot A. N. (2007) Chondrites and their components. In *Meteorites, Planets, and Comets*, edited by Davis A. M., Vol. 1 *Treatise on Geochemistry, Electronic Edition,* edited. Holland H. D. and Turekian K. K. Oxford: Elsevier (http://www.sciencedirect.com/science/referenceworks/9780080437514).

Stolper E. and Paque J. M. 1986. Crystallization sequences of Ca-Al-rich inclusions from Allende: the effects of cooling rate and maximum temperature. *Geochimica et Cosmochimica Acta* 50:1785–1806.

Taylor S., Alexander C.M.O'D, Delaney J., Ma P., Herzog G.F., and Engrand C. 2005. Isotopic fractionaiton of iron, potassium , and oxygen in stony cosmic sherules: Implications for heating histories and sources. *Geochimica et Cosmochimica Acta* 69:2647–2662.

Tsuchiyama A. and Fujimoto S. 1995. Evaporation experiments of metallic iron in vacuum. *Proc. NIPR Symposium on Antarctic Meteorites* 8:205-213.

Villeneuve J., Chaussidon M., and Libourel G. 2009. Homogeneous distribution of ^{26}Al in solar system from Mg isotopic composition of chondrules. *Science* 325:985-988.

Wang J., Davis A. M., Clayton R. N., Mayeda T. K. & Hashimoto A. 2001. Chemical and isotopic fractionation during the evaporation of the FeO-MgO-SiO_2-CaO-Al_2O_3-TiO_2-REE melt system. *Geochimica et Cosmochimica Acta* 65:479–494.

Weidenschilling S.J. 1977. Aerodynamics of solid bodies in solar nebula. *Monthly Notices of the Royal Astronomical Society* 180:57-80.

Williams R. J. and Mullins O. 1976. A system using solid ceramic oxygen electrolyte cells to measure oxygen fugacities in gas-mixing systems. *NASA Technical Memorandum* 58167.

Young E.D. 2000. Assessing the implications of K isotope cosmochemistry for evaporation of in the preplanetary solar nebula. *Earth & Planetary Science Letters* 183:321-333.

Yu Y. and Hewins R.H. 1997. Evaporation of potassium and sodium under vacuum conditions - Did chondrules really form at low pressure? *Lunar and Planetary Science* 28:1613-1614.

Yu Y., Hewins R. H., Alexander C. M. O'D., and Wang J. 2003. Experimental study of evaporation and isotopic mass fractionation of potassium in silicate melts. *Geochimica et Cosmochimica Acta* 67:773–786.

Zanda B. 2004. Chondrules. *Earth & Planetary Science Letters*. 224:1-17.

Zhu X.K., Guo Y., O'Nions R.K., Young E.D., and Ash R.D. 2001. Isotopic homogeneity of iron in the early solar nebula. *Nature* 412:311-313.